

# Tracking Drift: Variation-Aware Entropy Scheduling for Non-Stationary Reinforcement Learning

Tongxi Wang<sup>1</sup> Zhuoyang Xia<sup>1</sup> Xinran Chen<sup>1</sup> Shan Liu<sup>2</sup>

## Abstract

Real-world reinforcement learning often faces environment drift, but most existing methods rely on static entropy coefficients/target entropy, causing over-exploration during stable periods and under-exploration after drift (thus slow recovery), and leaving unanswered the principled question of how exploration intensity should scale with drift magnitude. We prove that entropy scheduling under non-stationarity can be reduced to a one-dimensional, round-by-round trade-off—faster tracking of the optimal solution after drift vs. avoiding gratuitous randomness when the environment is stable, so exploration strength can be driven by measurable online drift signals. Building on this, we propose AES (Adaptive Entropy Scheduling), which adaptively adjusts the entropy coefficient/temperature online using observable drift proxies during training, requiring almost no structural changes and incurring minimal overhead. Across 4 algorithm variants, 12 tasks, and 4 drift modes, AES significantly reduces the fraction of performance degradation caused by drift and accelerates recovery after abrupt changes.

## 1. Introduction

Reinforcement learning (RL) has achieved remarkable success across a wide range of domains (Sutton & Barto, 1998; Mnih et al., 2015). However, most existing theory and many practical algorithms are developed under a **stationarity assumption**, namely that the reward function and environment dynamics remain fixed over time. In real-world applications, this assumption is often violated: robots encounter changing physical conditions, autonomous driving systems must cope with evolving traffic patterns, and recommender systems are required to continuously adapt to shifting user preferences.

<sup>1</sup>School of Future Technology, Southeast University, Nanjing, China <sup>2</sup>School of Automation, Southeast University, Nanjing, China. Correspondence to: Shan Liu <liushan22@seu.edu.cn>.

Preprint. January 28, 2026.

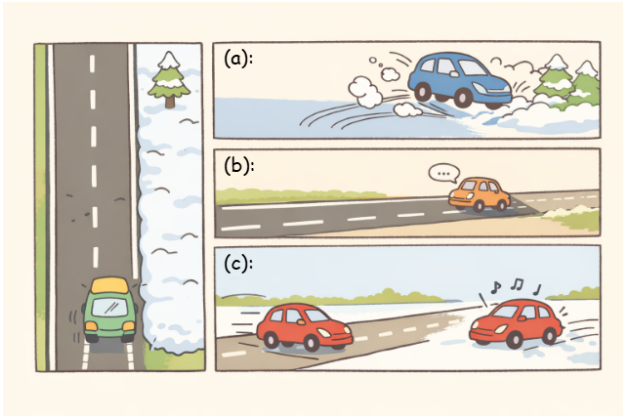


**Figure 1. Intuition for adaptive exploration in non-stationary environments.** The left panel illustrates an environment whose conditions evolve over time (e.g., changes in road conditions, friction, or task objectives). The right panels (a–c) contrast agent behaviors under different exploration regimes: (a) when abrupt environmental changes occur, insufficient exploration leads to delayed adaptation and poor recovery; (b) during stable periods, overly strong exploration introduces unnecessary randomness and degrades performance; (c) by adaptively adjusting exploration strength based on online drift signals, the agent can rapidly recover after changes while maintaining efficient exploitation in stable phases. This figure summarizes the core idea of the paper: treating exploration strength as a one-dimensional control variable driven by environmental drift, balancing fast tracking of changes against avoiding gratuitous randomness.

In such scenarios, an agent effectively interacts not with a single stationary Markov decision process (MDP), but with a **sequence of time-varying MDPs** (Uther, 2004; Besbes et al., 2014).

The central challenge of non-stationary reinforcement learning lies not only in learning an optimal policy, but also in **continuously adapting** to a changing environment while maintaining a balance between exploitation and exploration. Modern maximum-entropy reinforcement learning methods make this balance explicit through entropy regularization, where the entropy coefficient (or temperature parameter) serves as the primary control knob for exploration. In practice, however, this parameter is typically treated as stationary: it is either fixed or adjusted to match a target entropy designed for stationary objectives, as in standard Soft Actor-

Critic (SAC) style algorithms (Haarnoja et al., 2018). This practice has gradually fostered an implicit assumption that entropy control is largely orthogonal to non-stationarity. Yet this assumption breaks down precisely when the environment changes: excessive exploration wastes samples during stable periods, while insufficient exploration significantly slows policy recovery after changes occur.

This work focuses on a seemingly simple yet crucial question: **how should exploration intensity scale with the magnitude of environmental change?** Existing research on non-stationary reinforcement learning partially alleviates adaptation challenges, but does not directly answer this question. Change-point detection methods can provide theoretical guarantees (Mellor & Shapiro, 2013), but often introduce additional computational and design complexity that makes them difficult to integrate into real-time continuous-control systems. Sliding-window strategies rely on manually chosen window sizes and lack principled guidance in high-dimensional reinforcement learning pipelines (Besbes et al., 2014). Meta-learning approaches can accelerate adaptation across tasks (Bing et al., 2023; Liu et al., 2024), yet they do not explicitly characterize the relationship between the **rate of environmental variation** and the **optimal entropy scheduling strategy**. Meanwhile, theoretical analyses of entropy regularization have largely focused on stationary settings, providing limited guidance on whether—and how—exploration strength should increase as non-stationarity intensifies. As a result, entropy coefficients in practice are still commonly tuned heuristically, with performance that is highly environment-dependent.

Our key observation is that the necessity of entropy scheduling is **conceptually independent** of the specific algorithmic details of reinforcement learning. Once non-stationarity induces drift in the optimal comparator (e.g., the optimal policy or decision rule), the learner faces a fundamental per-round trade-off: (i) adapting sufficiently fast to track the drifting optimum, versus (ii) avoiding unnecessary randomness when the environment is stable. This perspective suggests that entropy control can be reduced to a **one-dimensional trade-off** that is sensitive to non-stationarity.

Based on this principle, we propose **Adaptive Entropy Scheduling (AES)**, a unified theoretical framework for non-stationary environments that adjusts the entropy coefficient online according to observable change signals. Our analysis yields a clear scaling prediction: dynamic performance loss is primarily governed by the interaction between the time horizon and the cumulative variation budget (Besbes et al., 2014; Cheung et al., 2020). More importantly, when applying this framework to deep reinforcement learning with function approximation and off-policy learning, we are able to explicitly distinguish the **dominant non-stationarity term** from **additional interface error terms**, thereby clar-

fying which factors must be controlled in practical training pipelines.

We instantiate AES as a plug-in entropy-scheduling mechanism for maximum-entropy reinforcement learning, resulting in **SAC+AES**, **PPO+AES**, **SQL+AES**, and **MEow+AES**. Across all carriers, the underlying learning algorithm is kept unchanged, and we only replace the fixed entropy weight (temperature  $\alpha$  or entropy-bonus coefficient) with the scheduled value produced by AES, without modifying the core actor-critic architecture. Entropy scheduling is driven by online signals already available during training, such as critic drift or, by default, a smoothed and clipped  $q$ -quantile ( $q = 0.9$ ) of absolute TD errors computed on the current update batch. We evaluate AES on three task families: Toy 2D multi-goal environment, MuJoCo continuous-control benchmarks, and large-scale Isaac Gym tasks under 4 drift modes, including abrupt, linear, periodic, and mixed changes induced by controlled goal, dynamics, or physics drifts. Across carriers and task suites, AES consistently mitigates performance degradation caused by non-stationarity and accelerates recovery after environmental changes compared to standard entropy-control baselines.

Overall, this work reveals a long-overlooked dimension of non-stationary deep reinforcement learning: **directly coupling exploration strength with online estimates of environmental variation through a tractable per-round trade-off**. We hope this perspective will move entropy scheduling beyond heuristic tuning toward variation-aware system design, and that it will integrate naturally with broader adaptive mechanisms in future research.

## 2. Related Work

### 2.1. Variation-Aware Non-Stationary RL

Non-stationary reinforcement learning (RL) is commonly formalized through variation budgets and dynamic regret, where rewards or transition dynamics evolve over time (Besbes et al., 2014). A growing body of recent work develops algorithms with guarantees that explicitly scale with the cumulative amount of non-stationarity. Model-free approaches show how policy updates should react to bounded variation in rewards and transitions (Mao et al., 2025; Peng & Papadimitriou, 2024), while complementary analyses extend these results to general function approximation and restart-based schemes (Feng et al., 2024). Empirical studies further confirm that fixed adaptation or exploration strategies are systematically suboptimal in drifting environments (Gregory Dal Toe et al., 2024; Hamadanian et al., 2025; Duan et al., 2025; Salaorni et al., 2025).

Together, these works establish a clear principle: optimal learning dynamics must explicitly depend on the rate of environmental change. However, existing variation-aware

analyses largely remain decoupled from modern maximum-entropy deep RL. In particular, they do not address how the entropy regularization coefficient—the primary exploration control knob in maximum-entropy methods—should be scheduled as a function of online non-stationarity. Our work directly targets this gap by reducing entropy control under non-stationarity to a one-dimensional, variation-sensitive trade-off derived from dynamic online optimization, and by instantiating this principle in entropy-regularized deep RL with explicit separation between the dominant non-stationarity term and additional interface errors.

## 2.2. Exploration Control: Entropy Scheduling vs. Heuristic Adaptation

Entropy-regularized RL, most notably Soft Actor-Critic (SAC) (Haarnoja et al., 2018), introduces an explicit entropy coefficient to balance exploration and exploitation. Classical analyses of entropy regularization focus primarily on stationary settings, characterizing how entropy decay or smoothing affects convergence and policy diversity, often yielding time-based schedules such as  $\mathcal{O}(t^{-1/2})$  (Szpruch et al., 2022; Jhaveri et al., 2025).

More recent work explores adaptive entropy mechanisms in complex domains, including distributed multi-agent RL (Hu et al., 2024) and large language model RL (Zhang et al., 2025). These approaches adjust entropy coefficients based on optimization dynamics or task difficulty, but they remain largely heuristic: the entropy parameter is tuned as an internal algorithmic quantity, without a principled link to the magnitude of environmental non-stationarity.

An alternative line of research addresses non-stationarity through explicit change-point detection and model or policy switching. Statistical testing and Bayesian schemes detect shifts in rewards, transitions, or value functions and trigger restarts or model reassignment (Alami et al., 2023; Chatrouny et al., 2025; Li et al., 2025). While such methods can precisely localize abrupt changes and achieve strong regret guarantees, they are often computationally heavy and treat exploration as secondary—typically fixed or adjusted implicitly via restarts—rather than continuously modulated in proportion to detected drift.

Meta-reinforcement learning and continual RL provide yet another adaptation paradigm, training agents to infer latent task structure or rapidly adapt across evolving environments (Bing et al., 2024; Qi et al., 2025; Khetarpal et al., 2022). Although effective at improving adaptability, these methods usually rely on fixed entropy regularization or ad-hoc noise injection, leaving exploration strength loosely coupled to the actual rate of environmental change.

In contrast to these approaches, our method provides a principled, lightweight mechanism for exploration control under

non-stationarity. The entropy coefficient is explicitly driven by an online non-stationarity proxy through a transparent per-round trade-off of the form  $C_1\alpha_t/\lambda_t + C_2\lambda_t$ , yielding a square-root-type scaling rule. This makes exploration strength increase when sustained drift is detected and decrease during stable phases, embedding adaptivity directly into the core learning rule rather than relying on heuristics, restarts, or learned adaptation alone.

## 3. Theory

This section states the minimal proof chain behind **Adaptive Entropy Scheduling (AES)** and explains how it connects to the drift signal used in our experiments. The key idea is that the entropy strength  $\lambda_t$  is a *one-dimensional control knob* balancing (i) **tracking** a drifting optimum and (ii) **stability** when the environment is quiet.

### 3.1. Dynamic mirror descent yields a per-round $\lambda$ -trade-off

We start from non-stationary online convex optimization (OCO) on the simplex  $\Pi = \Delta_K = \{x \in \mathbb{R}_+^K : \sum_{i=1}^K x_i = 1\}$ . At round  $t$ , the learner plays  $x_t \in \Pi$  and suffers a convex differentiable loss  $f_t$ . A *dynamic comparator* is a sequence  $\{u_t\}_{t=1}^T \subset \Pi$  with drift  $\alpha_t := \|u_t - u_{t-1}\|_1$  (set  $u_0 = u_1$ ), and dynamic regret

$$\text{Reg}_T^{\text{dyn}}(u_{1:T}) := \sum_{t=1}^T (f_t(x_t) - f_t(u_t)). \quad (1)$$

**Entropy mirror descent.** Let  $\Psi(x) := \sum_{i=1}^K x_i \log x_i$  be negative entropy. Define

$$D_\Psi(x, y) := \Psi(x) - \Psi(y) - \langle \nabla \Psi(y), x - y \rangle, \quad (2)$$

and the mirror-descent update

$$x_{t+1} = \arg \min_{x \in \Pi} \left\{ \eta_t \langle g_t, x \rangle + D_\Psi(x, x_t) \right\}. \quad (3)$$

We use the  $\ell_1/\ell_\infty$  pairing:  $\|\cdot\| = \|\cdot\|_1$  and  $\|\cdot\|_* = \|\cdot\|_\infty$ .

**Lemma 3.1** (Dynamic MD inequality). *Let  $\{u_t\}_{t=1}^T \subset \Pi$  be any comparator sequence and set  $u_0 = u_1$ . Assume bounded mirror gradients: there exists  $G_\Psi < \infty$  such that*

$$\|\nabla \Psi(z)\|_* \leq G_\Psi, \quad \forall z \in \Pi, \quad (4)$$

and assume  $\eta_t$  is nondecreasing. Then the iterates generated by (3) satisfy

$$\begin{aligned} \sum_{t=1}^T \langle g_t, x_t - u_t \rangle &\leq \frac{D_\Psi(u_1, x_1)}{\eta_1} + \sum_{t=1}^T \frac{\eta_t}{2} \|g_t\|_*^2 \\ &\quad + \sum_{t=2}^T \frac{2G_\Psi}{\eta_t} \|u_t - u_{t-1}\|_1. \end{aligned} \quad (5)$$

Appendix E provides a complete proof. This lemma is the main ‘‘non-stationary switch’’: it isolates drift through  $\sum_t \|u_t - u_{t-1}\|_1 / \eta_t$ .

**Entropy regularization and a master dynamic-regret inequality.** Assume bounded gradients for the base losses:

$$\|\nabla f_t(x)\|_\infty \leq G, \quad \forall x \in \Pi. \quad (6)$$

AES uses the time-varying regularized losses

$$\hat{f}_t(x) := f_t(x) + \lambda_t \Psi(x), \quad (7)$$

and runs (3) with  $g_t = \nabla \hat{f}_t(x_t)$ . Convexity gives

$$\hat{f}_t(x_t) - \hat{f}_t(u_t) \leq \langle \nabla \hat{f}_t(x_t), x_t - u_t \rangle. \quad (8)$$

Combining (8) with Lemma 3.1 yields

$$\begin{aligned} \sum_{t=1}^T (\hat{f}_t(x_t) - \hat{f}_t(u_t)) &\leq \frac{D_\Psi(u_1, x_1)}{\eta_1} + \sum_{t=1}^T \frac{\eta_t}{2} \|\nabla \hat{f}_t(x_t)\|_*^2 \\ &\quad + \sum_{t=2}^T \frac{2G_\Psi}{\eta_t} \|u_t - u_{t-1}\|_1. \end{aligned} \quad (9)$$

To remove regularization, use

$$f_t(x_t) - f_t(u_t) = (\hat{f}_t(x_t) - \hat{f}_t(u_t)) - \lambda_t (\Psi(x_t) - \Psi(u_t)), \quad (10)$$

and the entropy bound  $|\Psi(x)| \leq \log K$  (Appendix F), which implies

$$-\lambda_t (\Psi(x_t) - \Psi(u_t)) \leq 2\lambda_t \log K. \quad (11)$$

Altogether,

$$\begin{aligned} \text{Reg}^{\text{dyn}}_T(u_{1:T}) &\leq \frac{D_\Psi(u_1, x_1)}{\eta_1} + \sum_{t=1}^T \frac{\eta_t}{2} \|\nabla \hat{f}_t(x_t)\|_*^2 \\ &\quad + \sum_{t=2}^T \frac{2G_\Psi}{\eta_t} \|u_t - u_{t-1}\|_1 + 2 \log K \sum_{t=1}^T \lambda_t. \end{aligned} \quad (12)$$

**Coupling  $\eta_t$  and  $\lambda_t$  produces a per-round trade-off.** AES couples the learning rate and entropy strength:

$$\eta_t = c \lambda_t, \quad c > 0, \quad (13)$$

with  $\lambda_t \in [\lambda_{\min}, \lambda_{\max}]$  and  $\eta_t$  nondecreasing. Moreover, since  $\nabla \hat{f}_t = \nabla f_t + \lambda_t \nabla \Psi$ ,

$$\|\nabla \hat{f}_t(x_t)\|_\infty \leq G + \lambda_t G_\Psi. \quad (14)$$

For negative entropy,  $G_\Psi$  is bounded on a truncated simplex  $\Delta_{K,\varepsilon}$  (Appendix F):

$$G_\Psi = \sup_{x \in \Delta_{K,\varepsilon}} \|\nabla \Psi(x)\|_\infty \leq 1 + |\log \varepsilon|. \quad (15)$$

Substituting (13) and (14) into (12) and absorbing higher-order dependence through  $\lambda_t \leq \lambda_{\max}$  (Appendix G) yields:

**Theorem 3.2** ( $\lambda$ -trade-off dynamic regret bound). *Run mirror descent (3) on  $\hat{f}_t$  with (13). Then there exist constants  $C_0, C_1, C_2 > 0$  independent of  $T$  such that for any comparator sequence  $u_{1:T} \subset \Pi$ ,*

$$\begin{aligned} \text{Reg}^{\text{dyn}}_T(u_{1:T}) &\leq C_0 + \sum_{t=2}^T \left( C_1 \frac{\alpha_t}{\lambda_t} + C_2 \lambda_t \right), \\ \alpha_t &:= \|u_t - u_{t-1}\|_1. \end{aligned} \quad (16)$$

Equivalently, each round contributes

$$\varphi_t(\lambda) := C_1 \frac{\alpha_t}{\lambda} + C_2 \lambda, \quad \lambda > 0. \quad (17)$$

The first term is a **tracking cost** (large drift  $\alpha_t$  favors larger  $\lambda_t$ ), while the second is a **stability cost** (large  $\lambda_t$  over-smooths and harms instantaneous optimality).

**Oracle scale.**

**Theorem 3.3** (Per-round oracle optimal  $\lambda_t$ ). *For each  $t \geq 2$ , define*

$$\lambda_t^* = \arg \min_{\lambda > 0} \varphi_t(\lambda) = \sqrt{\frac{C_1}{C_2} \alpha_t}. \quad (18)$$

Then

$$\begin{aligned} \text{Reg}^{\text{dyn}}_T(u_{1:T}) &\leq C_0 + 2 \sqrt{C_1 C_2} \sum_{t=2}^T \sqrt{\alpha_t} \\ &\leq C_0 + 2 \sqrt{C_1 C_2} \sqrt{T \sum_{t=2}^T \alpha_t}. \end{aligned} \quad (19)$$

### 3.2. A fully-online schedule from an observable drift proxy

The oracle  $\lambda_t^*$  depends on  $\alpha_t$ , which is usually unobservable. AES instead assumes a proxy sequence  $\hat{\alpha}_t$  satisfying

$$\alpha_t \leq \hat{\alpha}_t, \quad (20)$$

and uses its prefix sum

$$\hat{A}_t := \sum_{s=1}^t \hat{\alpha}_s. \quad (21)$$

The resulting online schedule (before clipping) is

$$\lambda_t = \sqrt{\frac{C_1}{C_2}} \sqrt{\frac{\hat{A}_t}{t}}. \quad (22)$$

**Theorem 3.4** (Online AES scheduling driven by an observable proxy). *Under the conditions of Theorem 3.2, and assuming (20), choosing  $\lambda_t$  by (22) yields*

$$\text{Reg}^{\text{dyn}}_T \leq C_0 \log K + 4 \sqrt{C_1 C_2 T \hat{A}_T}. \quad (23)$$

In practice we clip  $\lambda_t$  to  $[\lambda_{\min}, \lambda_{\max}]$ :

$$\lambda_t = \text{clip}_{[\lambda_{\min}, \lambda_{\max}]} \left( \sqrt{\frac{C_1}{C_2}} \sqrt{\frac{\hat{A}_t}{t}} \right), \quad (24)$$

which introduces only controllable additive compensation terms (Appendix J).

### 3.3. Bridge to non-stationary maximum-entropy RL

We now show how MDP drift induces comparator drift, and why **critic drift** is a sensible proxy  $\hat{\alpha}_t$  in experiments.

**Non-stationary soft MDPs.** Let  $M_t = (\mathcal{S}, \mathcal{A}, P_t, r_t, \rho, \gamma)$  be a sequence of discounted MDPs with bounded rewards. For a policy  $\pi$ , define the maximum-entropy return  $J_t(\pi) = \mathbb{E}[\sum_{h \geq 0} \gamma^h (r_t(s_h, a_h) + \mu H(\pi(\cdot | s_h)))]$  and let  $\pi_t^* \in \arg \max_{\pi} J_t(\pi)$ .

**MDP variation controls  $Q^*$  drift.** Define the non-stationarity budget

$$B_T^{\text{MDP}} := \sum_{t=2}^T \left( \Delta_t^r + \gamma V_{\max} \Delta_t^P \right),$$

where  $\Delta_t^r := \sup_{s,a} |r_t(s, a) - r_{t-1}(s, a)|$  and  $\Delta_t^P := \sup_{s,a} \|P_t(\cdot | s, a) - P_{t-1}(\cdot | s, a)\|_1$ . Let  $Q_t^*$  be the soft-optimal  $Q$ -function. A standard fixed-point perturbation argument for the  $\gamma$ -contractive soft Bellman operator gives (Appendix K)

$$\|Q_t^* - Q_{t-1}^*\|_\infty \leq \frac{1}{1-\gamma} \left( \Delta_t^r + \gamma V_{\max} \Delta_t^P \right). \quad (25)$$

**$Q^*$  drift controls  $\pi^*$  drift.** For each  $s$ ,  $\pi_t^*(\cdot | s) = \text{softmax}(Q_t^*(s, \cdot) / \mu)$ . Using a statewise  $\ell_1 - \ell_\infty$  Lipschitz bound for softmax (Appendix L),

$$\|\pi_t^*(\cdot | s) - \pi_{t-1}^*(\cdot | s)\|_1 \leq \frac{1}{\mu} \|Q_t^* - Q_{t-1}^*\|_\infty. \quad (26)$$

Combining (25)–(26) shows that the comparator drift in the OCO view is controlled by  $B_T^{\text{MDP}}$  up to  $(\mu(1-\gamma))^{-1}$  factors.

**Why this matches the OCO surrogate.** For each state  $s$ , define the per-state linear-plus-entropy loss

$$f_{t,s}(\pi_s) := -\langle Q_t^*(s, \cdot), \pi_s \rangle + \mu \Psi(\pi_s), \quad \pi_s \in \Delta(\mathcal{A}).$$

The soft-optimal policy satisfies  $\pi_t^*(\cdot | s) = \arg \min_{\pi_s} f_{t,s}(\pi_s)$ , and the gap has an explicit KL form:

$$f_{t,s}(\pi(\cdot | s)) - f_{t,s}(\pi_t^*(\cdot | s)) = \mu \text{KL}(\pi(\cdot | s) \| \pi_t^*(\cdot | s)).$$

Thus, the principal term in soft-RL dynamic regret is an occupancy-weighted sum of per-state OCO regrets with comparator  $u_{t,s} = \pi_t^*(\cdot | s)$ .

**Overall (planning-version) rate.**

**Theorem 3.5** (AES-RL-Plan: non-stationary soft-RL dynamic regret (principal term)). *In a non-stationary tabular soft-MDP sequence, run AES with the online schedule from Theorem 3.4 using a valid drift proxy. Then there exists a constant  $C$  such that*

$$\text{Reg}_T^{\text{RL}} \leq \tilde{O} \left( \frac{\sqrt{|\mathcal{S}| \log |\mathcal{A}|}}{\mu(1-\gamma)^2} \sqrt{B_T^{\text{MDP}} T} \right) + \sum_{t=1}^T \text{Bias}_t,$$

where  $\text{Bias}_t$  collects planning-to-RL interface residuals (made explicit in the appendix).

**From planning to learning.** Theorems such as Theorem 3.5 are stated in an “ideal” (planning/full-information) form to expose the dominant non-stationarity dependence. In practical off-policy RL with function approximation, two additional effects appear: (i)  **$Q^*$ -substitution/approximation** (we use a learned critic  $Q_{\theta_t}$  instead of  $Q_t^*$ ), and (ii) **occupancy mismatch** (updates are weighted by a replay/on-policy distribution rather than  $d_t^{\pi_t^*}$ ). Appendices N/O give an explicit decomposition that upper bounds the per-round gap by the ideal OCO term plus additive bias/mismatch terms; in Theorem 3.5 they are collected into  $\text{Bias}_t$ .

### 3.4. Experiment-Theory Interface.

Our theoretical analysis characterizes entropy scheduling under non-stationarity as a per-round trade-off between tracking a drifting optimum and avoiding excessive randomness. This yields an oracle scaling law of the form  $\lambda_t^* \propto \sqrt{\alpha_t}$ , where  $\alpha_t$  denotes the (unobservable) drift of the optimal comparator.

In practical reinforcement learning,  $\alpha_t$  cannot be accessed directly. Importantly, the theory does not require exact knowledge of  $\alpha_t$ . It only assumes the availability of an online proxy that upper-bounds or correlates monotonically with the underlying comparator drift. Accordingly, in our experiments we instantiate AES using critic-based drift signals, such as high quantiles of absolute TD errors, which empirically increase following environmental changes and decay during stable phases.

The goal of our experiments is therefore not to empirically verify regret bounds, but to test the structural prediction implied by the theory: that exploration strength should increase when non-stationarity intensifies and decrease when the environment stabilizes. Metrics such as recovery speed after abrupt changes, performance drop area ratio, and normalized AUC serve as behavioral indicators of how effectively the scheduled entropy adapts to environmental drift in deep reinforcement learning systems.

Table 1. How AES is integrated into each algorithm carrier. We keep the base algorithms unchanged except for replacing the entropy weight with the scheduled value.

Carrier	Entropy weight	AES output and injection	Default proxy
SAC	temperature $\alpha$	output $\alpha_t$ ; replace $\alpha$ in the actor objective term $\alpha_t \log \pi(a s)$ (and the corresponding soft target/value computation, if applicable)	$\text{Quantile}_{0.9}( \delta^{Q_1}  \cup  \delta^{Q_2} )$ + smoothing
PPO	entropy coefficient $c_{\text{ent}}$	output $c_{\text{ent},t}$ ; replace $c_{\text{ent}}$ in the policy loss term $-c_{\text{ent},t} H(\pi(\cdot s))$	$\text{Quantile}_{0.9}( \delta^V )$ over rollout batch + smoothing
SQL	temperature $\alpha$	output $\alpha_t$ ; replace $\alpha$ in soft backup/value computation (soft Bellman target)	$\text{Quantile}_{0.9}( \delta^{\text{soft}Q} )$ + smoothing
MEow	temperature $\alpha$	output $\alpha_t$ ; replace $\alpha$ wherever it appears in the clipped double- $Q$ targets / soft value computation; synchronize online/target modules	$\text{Quantile}_{0.9}( \delta^{Q_1}  \cup  \delta^{Q_2} )$ + smoothing (EMA recommended)

## 4. Experiments

### 4.1. Experiment Setup

**Algorithm carriers.** We evaluate AES on four maximum-entropy RL algorithms: SAC (Haarnoja et al., 2018), PPO (Schulman et al., 2017), SQL (Haarnoja et al., 2017), and MEow (Chao et al., 2024). All methods contain an explicit entropy regularization term (temperature  $\alpha$  for SAC/SQL/MEow, entropy bonus  $c_{\text{ent}}$  for PPO). AES is integrated without modifying the underlying actor-critic or value-learning structure, covering both off-policy and on-policy learning as well as distinct MaxEnt formulations. For the SAC baseline, we applied automatic temperature control. So SAC and MEow are considered as strong baselines.

AES acts as a plug-in exploration controller that schedules the entropy weight online. At each update, a scalar drift proxy is extracted from critic TD errors (off-policy) or value TD deltas (PPO), smoothed via a window or EMA, and fed into the variation-aware scheduler. AES outputs a scheduled temperature  $\alpha_t$  (SAC/SQL/MEow) or entropy coefficient  $c_{\text{ent},t}$  (PPO), replacing the fixed entropy weight. Our default proxy is the  $q$ -quantile of absolute TD errors,

$$\hat{\alpha}_t = \text{Quantile}_q(|\delta|), \quad q = 0.9, \quad (27)$$

computed on the current update batch. The scheduled entropy weight is clipped to a fixed range for numerical stability. Carrier-specific injection points are summarized in Table 1. We emphasize that AES does not rely on TD errors being accurate estimators of the true comparator drift; any proxy whose magnitude correlates monotonically with changes in the learning dynamics is sufficient to instantiate the scheduling principle.

**Tasks and non-stationarity.** We evaluate AES on three task families: **Toy** (2D multi-goal), **MuJoCo** (Todorov et al., 2012) (Hopper, HalfCheetah, Walker2d, Ant, Humanoid), and **Isaac Gym** (Makoviychuk et al., 2021) (Ant, Humanoid, Ingenuity, ANYmal, AllegroHand, FrankaCabinet). Each

task is trained under five non-stationarity patterns: *Steady*, *Abrupt*, *Linear*, *Periodic*, and *Mixed*. Drifts are injected via goal changes (Toy), dynamics or target variations (MuJoCo), and scalable physics or task perturbations (Isaac Gym). Change points are aligned by training progress to ensure comparability.

**Evaluation protocol.** All results are averaged over multiple random seeds with appropriate dispersion. Methods are aligned by environment interaction steps and evaluated under identical drift schedules and termination criteria. AES incurs negligible overhead, requiring only a scalar statistic of TD errors and a lightweight scheduler update per iteration.

Unlike change-point detection or restart-based methods, AES performs continuous entropy modulation and does not explicitly detect or localize change points.

### 4.2. Evaluation Metrics

We report three complementary metrics that jointly capture overall sample efficiency, robustness to non-stationarity, and direct post-change adaptation speed.

**(1) Normalized AUC.** For each method and task, we compute the area under the return-environment-steps curve

$$\text{AUC} = \int_0^T R(t) dt, \quad (28)$$

where  $R(t)$  is the expected return at environment step  $t$  and  $T$  is the total training steps. To reduce scale differences across tasks, we normalize AUC by the **Steady SAC** baseline within the same task family  $\mathcal{F}$ :

$$\text{nAUC}(\tau) = \frac{\text{AUC}(\tau)}{\text{AUC}(\text{SAC, Steady, } \mathcal{F})}. \quad (29)$$

**(2) Performance drop area ratio.** To quantify the proportion of performance loss induced by non-stationarity, we

Table 2. Overall performance under different non-stationarity patterns. We report normalized AUC (higher is better) and performance drop area ratio (lower is better) for each method across five change patterns (Steady, Abrupt, Linear, Periodic, Mixed), aggregated within each task family. Normalization is performed relative to the Steady SAC baseline in the same family.

	nAUC $\uparrow$					Performance drop area ratio $\downarrow$				
	Steady	Abrupt	Linear	Periodic	Mixed	Steady	Abrupt	Linear	Periodic	Mixed
Toy										
SAC	1.00	0.72	0.80	0.81	0.73	0.00	0.28	0.20	0.19	0.27
PPO	0.89	0.75	0.79	0.71	0.67	0.00	0.16	0.11	0.20	0.25
SQL	0.90	0.75	0.82	0.77	0.68	0.00	0.17	0.09	0.14	0.24
MEow	0.90	0.79	0.87	0.86	0.77	0.00	0.12	0.03	0.04	0.14
SAC+AES	<b>1.13</b>	0.88	0.94	0.94	<b>0.97</b>	0.00	0.22	0.17	0.17	0.14
PPO+AES	0.89	0.92	0.92	0.89	0.79	0.00	-0.03	-0.03	0.00	0.11
SQL+AES	0.98	0.90	0.94	0.93	0.91	0.00	0.08	0.04	0.05	<b>0.07</b>
MEow+AES	0.97	<b>1.03</b>	<b>1.02</b>	<b>1.01</b>	0.83	0.00	<b>-0.06</b>	<b>-0.05</b>	<b>-0.04</b>	0.14
MuJoCo	Steady	Abrupt	Linear	Periodic	Mixed	Steady	Abrupt	Linear	Periodic	Mixed
SAC	1.00	0.67	0.76	0.68	0.65	0.00	0.33	0.24	0.32	0.35
PPO	0.88	0.66	0.64	0.67	0.57	0.00	0.25	0.27	0.24	0.35
SQL	0.80	0.52	0.53	0.50	0.44	0.00	0.35	0.34	0.38	0.45
MEow	0.92	0.67	0.71	0.79	0.63	0.00	0.27	0.23	0.14	0.32
SAC+AES	<b>1.24</b>	0.87	<b>0.94</b>	<b>0.94</b>	<b>0.94</b>	0.00	0.30	0.24	0.24	0.24
PPO+AES	0.94	0.69	0.79	0.82	0.77	0.00	0.27	0.16	0.13	0.18
SQL+AES	0.81	0.65	0.79	0.71	0.64	0.00	0.20	<b>0.02</b>	0.12	0.21
MEow+AES	0.98	<b>0.95</b>	0.88	0.87	0.89	0.00	<b>0.03</b>	0.10	<b>0.11</b>	<b>0.09</b>
Isaac Gym	Steady	Abrupt	Linear	Periodic	Mixed	Steady	Abrupt	Linear	Periodic	Mixed
SAC	1.00	0.58	0.69	0.57	0.51	0.00	0.42	0.31	0.43	0.49
PPO	0.82	0.44	0.59	0.55	0.48	0.00	0.46	0.28	0.33	0.41
SQL	0.76	0.39	0.47	0.49	0.38	0.00	0.49	0.38	0.36	0.50
MEow	0.99	0.68	0.76	0.76	0.54	0.00	0.31	0.23	0.23	0.45
SAC+AES	<b>1.13</b>	0.73	<b>0.93</b>	0.95	0.79	0.00	0.35	0.18	0.16	0.30
PPO+AES	0.87	0.62	0.67	0.70	0.57	0.00	0.29	0.23	0.20	0.34
SQL+AES	0.81	0.66	0.66	0.72	0.60	0.00	<b>0.19</b>	0.19	0.11	0.26
MEow+AES	1.09	<b>0.81</b>	0.90	<b>0.99</b>	<b>0.92</b>	0.00	0.26	<b>0.17</b>	<b>0.09</b>	<b>0.16</b>

compare the AUC under a non-stationary pattern to the corresponding Steady AUC. Let  $AUC^{ns}$  be the AUC under a non-stationary pattern and  $AUC^{steady}$  the AUC under Steady. We define

$$\text{DropRatio} = 1 - \frac{AUC^{ns}}{AUC^{steady}}. \quad (30)$$

Smaller values indicate less cumulative damage from drift.

**(3) Abrupt-change recovery time.** Under the **Abrupt** pattern, we measure how quickly a method recovers after a change point. Specifically, recovery time is defined as the number of environment steps from the change occurrence to the first time the performance returns to the pre-change level (using the same evaluation protocol as the learning curves). We report recovery time *normalized* by the total training steps, so the metric is comparable across tasks.

Let  $\{t_{\text{change}}^{(i)}\}_{i=1}^K$  denote the set of  $K$  change points during training, and let  $t_{\text{recover}}^{(i)}$  be the corresponding recovery time after the  $i$ -th change. We define the normalized recovery time as

$$\text{Rec}(\tau) = \frac{1}{T} \sum_{i=1}^K \left( t_{\text{recover}}^{(i)} - t_{\text{change}}^{(i)} \right), \quad (31)$$

Lower recovery ratios indicate stronger adaptability to abrupt non-stationarity. where  $T$  is the total number of training steps.

#### 4.3. Overall Performance Across Non-stationarity Patterns

We first evaluate overall performance under five patterns (Steady, Abrupt, Linear, Periodic, Mixed) across three task

Table 3. **Adaptation speed after abrupt environmental changes.** Abrupt-change recovery time is reported as the fraction of total training steps required for performance to return to the pre-change level after each change point. Lower values indicate better adaptability.

Abrupt-change recovery time									
Family	Task	SAC	PPO	SQL	MEow	SAC +AES	PPO +AES	SQL +AES	MEow +AES
Toy	2d multi-goal	7.8%	7.6%	9.4%	6.1%	3.7%	3.7%	4.6%	3.2%
MuJoCo	Hopper	12.2%	9.4%	12.7%	10.9%	6.4%	6.1%	6.6%	4.7%
	HalfCheetah	9.6%	8.0%	11.8%	7.7%	5.1%	5.1%	5.8%	4.4%
	Walker2d	10.9%	9.0%	12.2%	9.0%	5.6%	5.5%	6.6%	4.7%
	Ant	11.9%	10.9%	16.4%	11.7%	6.7%	6.9%	8.3%	5.9%
	Humanoid	14.8%	13.0%	16.3%	15.1%	8.6%	10.3%	10.6%	7.5%
Isaac Gym	Ant	14.1%	11.2%	17.5%	11.6%	8.7%	9.7%	10.2%	7.0%
	Humanoid	16.5%	14.1%	18.2%	12.5%	9.8%	10.5%	13.9%	7.8%
	Ingenuity	15.3%	14.1%	16.7%	12.7%	8.2%	11.0%	11.6%	7.0%
	ANYmal	13.5%	13.8%	17.7%	12.5%	9.0%	8.7%	10.2%	6.5%
	AllegroHand	21.5%	18.4%	21.3%	14.6%	10.6%	12.1%	14.6%	9.8%
	FrankaCabinet	19.4%	15.9%	18.5%	14.6%	10.5%	11.6%	13.7%	8.5%

families (Toy, MuJoCo, Isaac Gym) and four algorithmic carriers (SAC, PPO, SQL, MEow). Table 2 summarizes **normalized AUC** and **drop-area ratio**.

**Overall trends.** Table 2 reveals a consistent benefit of AES across task families and carriers. Under **non-stationary patterns** (Abrupt/Linear/Periodic/Mixed), AES generally *increases* normalized AUC while *reducing* the drop-area ratio, indicating improved sample efficiency and stronger robustness to changes. Under the **Steady** pattern, we do not observe systematic degradation; in most settings the normalized AUC is comparable or slightly improved. This suggests that AES is not a one-off patch specialized for change events, but rather a broadly applicable mechanism for *adaptive calibration of exploration strength*.

#### 4.4. Abrupt-change Recovery Time

We next focus on adaptation speed under abrupt non-stationarity. Table 3 reports the **normalized abrupt-change recovery time** (percentage of total training steps) across all tasks and carriers.

**Recovery is consistently faster with AES.** Across all tasks and carriers, AES reduces normalized recovery time. Averaged over the 12 tasks, recovery time decreases from  $\approx 13.96\%$  to  $7.74\%$  for SAC, from  $\approx 12.12\%$  to  $8.43\%$  for PPO, from  $\approx 15.73\%$  to  $9.73\%$  for SQL, and from  $\approx 11.58\%$  to  $6.42\%$  for MEow. Gains are especially large on high-dimensional tasks (e.g., ALLEGROHAND and FRANKACABINET), where distribution shifts are more disruptive, consistent with the role of increased exploration after change points.

#### 4.5. Summary

Combining Sheet 1 (normalized AUC and drop-area ratio) with Sheet 2 (abrupt-change recovery time), we observe three key characteristics of AES: **(i) Cross-algorithm consistency:** all four carriers benefit, suggesting that AES functions as a *plug-in exploration-strength control layer*. **(ii) Stronger gains under more severe or composite changes:** improvements are most pronounced under Abrupt and Mixed patterns, where changes are sharper and harder to track, as reflected by larger reductions in drop-area ratio and recovery time. **(iii) Good steady-state behavior:** under Steady training, we do not see systematic regressions, alleviating the common concern that better adaptation to non-stationarity must come at the cost of stable-phase performance. Ablation study is shown in Appendix Q.

## 5. Conclusion

This work theoretically characterizes entropy scheduling in non-stationary reinforcement learning as a “one-dimensional, round-by-round trade-off,” and, based on this view, proposes AES, which adaptively adjusts the entropy coefficient/temperature online using observable drift proxy signals, substantially reducing drift-induced performance degradation and accelerating recovery after abrupt changes across multiple algorithms, tasks, and drift modes.

Future research could explore engineering implementation methods that better align with the theoretical boundaries presented in this paper, investigate more agent selection methods, or provide theoretical extensions for continuous control tasks.

## Impact Statement

This paper presents work whose goal is to advance the field of Machine Learning. There are many potential societal consequences of our work, none which we feel must be specifically highlighted here.

## References

Alami, R., Raj, A., and Moulines, É. Restarted bayesian online change-point detection for non-stationary markov decision processes. In *Proceedings of the 40th International Conference on Machine Learning*, volume 202 of *Proceedings of Machine Learning Research*, 2023.

Besbes, O., Gur, Y., and Zeevi, A. Stochastic multi-armed-bandit problem with non-stationary rewards. In *Advances in Neural Information Processing Systems 27*, pp. 199–207, 2014.

Bing, Z., Knak, L., Cheng, L., Morin, F. O., Huang, K., and Knoll, A. Meta-reinforcement learning in nonstationary and nonparametric environments. *IEEE Transactions on Neural Networks and Learning Systems*, 34(12):10667–10680, 2023. doi: 10.1109/TNNLS.2023.3270298.

Bing, Z., Knak, L., Cheng, L., Morin, F. O., Huang, K., and Knoll, A. Meta-reinforcement learning in nonstationary and nonparametric environments. *IEEE Transactions on Neural Networks and Learning Systems*, 35(10):13604–13618, 2024. doi: 10.1109/TNNLS.2023.3270298.

Chao, C.-H., Feng, C., Sun, W.-F., Lee, C.-K., See, S., and Lee, C.-Y. Maximum entropy reinforcement learning via energy-based normalizing flow. *Advances in Neural Information Processing Systems*, 37:56136–56165, 2024.

Chartouny, A., Khamassi, M., and Girard, B. Multi-model reinforcement learning with online retrospective change-point detection. *bioRxiv*, 2025. doi: 10.1101/2025.05.13.653727.

Cheung, W. C., Simchi-Levi, D., and Zhu, R. Reinforcement learning for non-stationary Markov decision processes: The blessing of (more) optimism. In *Proceedings of the 37th International Conference on Machine Learning*, volume 119 of *Proceedings of Machine Learning Research*, pp. 1843–1854. PMLR, 2020.

Duan, T., Zhang, Z., Guo, S., Zhao, Y., Lin, Z., Fang, Z., Liu, Y., Luan, D., Huang, D., and Cui, Y. Sample efficient experience replay in non-stationary environments. *arXiv preprint arXiv:2509.15032*, 2025.

Feng, S., Yin, M., Huang, R., Wang, Y.-X., Yang, J., and Liang, Y. Towards general function approximation in nonstationary reinforcement learning. In *2024 IEEE International Symposium on Information Theory (ISIT)*, 2024.

Gregory Dal Toe, S., Tiddeman, B., and MacParthaláin, N. Towards reinforcement learning for non-stationary environments. In *Proceedings of the 22nd UK Workshop on Computational Intelligence*, 2024.

Haarnoja, T., Tang, H., Abbeel, P., and Levine, S. Reinforcement learning with deep energy-based policies. In *International conference on machine learning*, pp. 1352–1361. PMLR, 2017.

Haarnoja, T., Zhou, A., Abbeel, P., and Levine, S. Soft actor-critic: Off-policy maximum entropy deep reinforcement learning with a stochastic actor. In *Proceedings of the 35th International Conference on Machine Learning*, pp. 1861–1870, 2018.

Hamadanian, P., Nasr-Esfahany, A., Schwarzkopf, M., Sen, S., and Alizadeh, M. Online reinforcement learning in non-stationary context-driven environments. In *Proceedings of the International Conference on Learning Representations*, 2025. LCPO.

Hu, Y., Fu, J., Wen, G., Lv, Y., and Ren, W. Distributed entropy-regularized multi-agent reinforcement learning with policy consensus. *Automatica*, 164:111652, 2024. doi: 10.1016/j.automatica.2024.111652.

Jhaveri, Y., Wiltzer, H., Shafto, P., Bellemare, M. G., and Meger, D. Convergence theorems for entropy-regularized and distributional reinforcement learning. *arXiv preprint arXiv:2510.08526*, 2025.

Khetarpal, K., Riemer, M., Rish, I., and Precup, D. Towards continual reinforcement learning: A review and perspectives. *Journal of Artificial Intelligence Research*, 75:1401–1476, 2022.

Li, M., Shi, C., Wu, Z., and Fryzlewicz, P. Testing stationarity and change point detection in reinforcement learning. *Annals of Statistics*, 53(3), 2025. doi: 10.1214/25-AOS2501.

Liu, Z., Zhao, Y., Li, J., and Zhang, T. Meta-reinforcement learning under non-stationarity: A dynamic adaptation perspective. In *Proceedings of the 41st International Conference on Machine Learning (ICML)*, 2024.

Makoviychuk, V., Wawrzyniak, L., Guo, Y., Lu, M., Storey, K., Macklin, M., Hoeller, D., Rudin, N., Allshire, A., Handa, A., et al. Isaac gym: High performance gpu based physics simulation for robot learning. In *NeurIPS Datasets and Benchmarks*, 2021.

Mao, W., Zhang, K., Zhu, R., Simchi-Levi, D., and Başar, T. Model-free nonstationary reinforcement learning: Near-optimal regret and applications in multiagent reinforcement learning and inventory control. *Management Science*, 71(2):1564–1580, 2025. doi: 10.1287/mnsc.2022.02533.

Mellor, J. and Shapiro, M. Change detection in mdps using bayesian methods. In *Advances in Neural Information Processing Systems*, 2013.

Mnih, V., Kavukcuoglu, K., Silver, D., Rusu, A. A., Veness, J., Bellemare, M. G., Graves, A., Riedmiller, M. A., Fidjeland, A., Ostrovski, G., Petersen, S., Beattie, C., Sadik, A., Antonoglou, I., King, H., Kumaran, D., Wierstra, D., Legg, S., and Hassabis, D. Human-level control through deep reinforcement learning. *Nature*, 518:529–533, 2015. URL <https://doi.org/10.1038/nature14236>.

Peng, B. and Papadimitriou, C. The complexity of non-stationary reinforcement learning. In *Proceedings of the 35th International Conference on Algorithmic Learning Theory*, volume 237 of *Proceedings of Machine Learning Research*, 2024.

Qi, C., Li, H., and Huang, P. Timrl: A novel meta-reinforcement learning framework for non-stationary and multi-task environments. *arXiv preprint arXiv:2501.07146*, 2025.

Salaorni, D., De Paola, V., Delpero, S., Dispoto, G., Bonetti, P., Russo, A., Calcagno, G., Trovò, F., Papini, M., Metelli, A. M., Mussi, M., and Restelli, M. Gym4real: A suite for benchmarking real-world reinforcement learning. *arXiv preprint arXiv:2507.00257*, 2025.

Schulman, J., Wolski, F., Dhariwal, P., Radford, A., and Klimov, O. Proximal policy optimization algorithms. *arXiv preprint arXiv:1707.06347*, 2017.

Sutton, R. S. and Barto, A. Reinforcement learning: An introduction. *IEEE Trans. Neural Networks*, 9:1054–1054, 1998. URL <https://doi.org/10.1109/TNN.1998.712192>.

Szpruch, Ł., Treetanthiploet, T., and Zhang, Y. Optimal scheduling of entropy regulariser for continuous-time linear-quadratic reinforcement learning. *SIAM Journal on Control and Optimization*, 2022. arXiv:2208.04466.

Todorov, E., Erez, T., and Tassa, Y. Mujoco: A physics engine for model-based control. In *2012 IEEE/RSJ international conference on intelligent robots and systems*, pp. 5026–5033. IEEE, 2012.

Uther, W. T. B. Markov decision processes. In *Encyclopedia of Machine Learning and Data Mining*, 2004. URL [https://doi.org/10.1007/978-1-4899-7687-1\\_512](https://doi.org/10.1007/978-1-4899-7687-1_512).

Zhang, X., Yuan, X., Huang, D., You, W., Hu, C., Ruan, J., Chen, K., and Hu, X. Rediscovering entropy regularization: Adaptive coefficient unlocks its potential for llm reinforcement learning. *arXiv preprint arXiv:2510.10959*, 2025.

## A. Notation, Norms, and Technical Preliminaries

### A.1. The simplex and the $\ell_1/\ell_\infty$ duality

**Simplex and truncated simplex.** For probability vectors of dimension  $K$ , define the simplex

$$\Delta_K := \left\{ x \in \mathbb{R}_+^K : \sum_{i=1}^K x_i = 1 \right\} \quad (32)$$

Several arguments require working on a truncated (or smoothed) simplex

$$\Delta_{K,\varepsilon} := \{x \in \Delta_K : x_i \geq \varepsilon, \forall i \in [K]\}, \quad \varepsilon \in (0, 1/K]. \quad (33)$$

A typical choice is  $\varepsilon = \Theta(T^{-2})$ , which only affects logarithmic factors; see Appendix A.3.

**Norm convention and duality.** The analysis uses

$$|x|_1 := \sum_{i=1}^K |x_i|, \quad |x|_\infty := \max_{i \in [K]} |x_i|. \quad (34)$$

They are dual norms. In particular, for any  $x, y \in \mathbb{R}^K$ , Hölder's inequality yields

$$\langle x, y \rangle \leq |x|_1 |y|_\infty, \quad \langle x, y \rangle \leq |x|_\infty |y|_1. \quad (35)$$

This pairing is natural for negative-entropy mirror descent on  $\Delta_K$ : path variation of comparators is measured in  $|\cdot|_1$ , while gradients are controlled in  $|\cdot|_\infty$ .

### A.2. Negative entropy: properties and Bregman identities

**Definition.** Let  $\log$  denote the natural logarithm. Define the negative entropy on  $\Delta_K$ :

$$\Psi(x) := \sum_{i=1}^K x_i \log x_i, \quad x \in \Delta_K, \quad (36)$$

with the standard convention  $0 \log 0 := 0$ . Thus  $\Psi(x) = -H(x)$  where  $H$  is Shannon entropy.

**Boundedness on  $\Delta_K$ .** For all  $x \in \Delta_K$ ,

$$-\log K \leq \Psi(x) \leq 0. \quad (37)$$

The minimum is attained at the uniform distribution  $x = \mathbf{1}/K$ , giving  $\Psi(\mathbf{1}/K) = -\log K$ , and the maximum is attained at vertices, where  $\Psi(e_j) = 0$ .

**Bregman divergence equals KL divergence.** The Bregman divergence induced by  $\Psi$  is

$$D_\Psi(x, y) := \Psi(x) - \Psi(y) - \langle \nabla \Psi(y), x - y \rangle. \quad (38)$$

For  $x, y \in \Delta_K$  (with the usual convention that the divergence is  $+\infty$  if  $y_i = 0$  but  $x_i > 0$ ),

$$D_\Psi(x, y) = \text{KL}(x|y) := \sum_{i=1}^K x_i \log \frac{x_i}{y_i}. \quad (39)$$

Hence  $D_\Psi(x, y) \geq 0$  and equals 0 iff  $x = y$ .

**Strong convexity w.r.t.  $|\cdot|_1$ .** Negative entropy is 1-strongly convex with respect to  $|\cdot|_1$  on  $\Delta_K$  in the following standard form:

$$\Psi(x) \geq \Psi(y) + \langle \nabla \Psi(y), x - y \rangle + \frac{1}{2} |x - y|_1^2, \quad \forall x, y \in \Delta_K. \quad (40)$$

Equivalently,

$$D_\Psi(x, y) \geq \frac{1}{2} |x - y|_1^2. \quad (41)$$

A convenient route is Pinsker's inequality, which implies  $\text{KL}(x|y) \geq \frac{1}{2} |x - y|_1^2$ .

**Bregman identities.** Two standard identities are repeatedly used.

- **Three-point identity.** For any  $a, b, c$  in the domain of  $\Psi$ ,

$$\langle \nabla \Psi(b) - \nabla \Psi(c), , a - b \rangle D_\Psi(a, c) - D_\Psi(a, b) - D_\Psi(b, c). \quad (42)$$

- **Add–subtract decomposition.** For any  $a, b, c$ ,

$$D_\Psi(a, c) - D_\Psi(a, b) \langle \nabla \Psi(b) - \nabla \Psi(c), , a - b \rangle + D_\Psi(b, c), \quad (43)$$

which follows directly from (A.2).

### A.3. Truncated/smoothed simplex: bounded gradients and curvature

Negative entropy has a technical singularity: if some coordinate approaches 0, then  $\log x_i \rightarrow -\infty$ , so  $\Psi$  is no longer Lipschitz and  $|\nabla \Psi(x)|_\infty$  becomes unbounded. This affects: (i) controlling constants through  $\sup_{x \in \Pi} |\nabla \Psi(x)|_\infty$ ; and (ii) any use of smoothness/curvature upper bounds.

A standard remedy is to work on  $\Delta_{K,\varepsilon}$  or equivalently apply a small smoothing to the iterates.

**Gradient bound on  $\Delta_{K,\varepsilon}$ .** For  $x \in \Delta_{K,\varepsilon}$ , all coordinates are positive and

$$\frac{\partial \Psi(x)}{\partial x_i} = 1 + \log x_i. \quad (44)$$

Since  $\varepsilon \leq x_i \leq 1$ , it holds that  $\log \varepsilon \leq \log x_i \leq 0$ , hence

$$|\nabla \Psi(x)|_\infty \leq 1 + |\log \varepsilon|. \quad (45)$$

**Hessian/curvature bound on  $\Delta_{K,\varepsilon}$ .** On  $\Delta_{K,\varepsilon}$ ,

$$\nabla^2 \Psi(x) = \text{diag}\left(\frac{1}{x_1}, \dots, \frac{1}{x_K}\right), \quad \text{so} \quad |\nabla^2 \Psi(x)|_{\text{op}} \leq \frac{1}{\varepsilon}. \quad (46)$$

Thus  $\Psi$  is  $1/\varepsilon$ -smooth in Euclidean geometry; when needed, norm conversions can translate this into the appropriate  $\ell_1/\ell_\infty$  constants.

**Algorithmic realizations.** Two equivalent implementation patterns are common:

- **Hard projection:** project each iterate back to  $\Delta_{K,\varepsilon}$  (e.g., clip small coordinates and renormalize).
- **Smoothing:** replace an output distribution  $\pi$  by  $(1 - \xi)\pi + \xi \mathbf{1}/K$  with tiny  $\xi$ , which guarantees  $\pi_i \geq \xi/K$ .

Both only introduce logarithmic factors (via  $|\log \varepsilon|$ ) and do not change the main rates.

## B. Complete Theory Chain

### B.1. Preliminaries and Problem Setting: a Unified View of OCO and Non-stationary Maximum-Entropy RL

This section studies adaptive exploration–exploitation in **non-stationary** environments. A fixed entropy regularization weight (temperature) may systematically mis-balance adaptation speed and excessive randomness when the environment varies over time. The analysis develops an **Adaptive Entropy Scheduling** (AES) principle: the entropy strength is scheduled online according to the magnitude of non-stationarity, yielding a unified theory chain from Online Convex Optimization (OCO) to non-stationary maximum-entropy reinforcement learning (soft-RL).

### B.1.1. NON-STATIONARY ONLINE CONVEX OPTIMIZATION (OCO)

The decision set is the  $K$ -dimensional simplex

$$\Pi = \Delta_K := \left\{ x \in \mathbb{R}_+^K : \sum_{i=1}^K x_i = 1 \right\}.$$

At round  $t = 1, \dots, T$ , the environment reveals a convex differentiable loss  $f_t : \Pi \rightarrow [0, 1]$ . Assume bounded gradients: there exists  $G > 0$  such that for all  $x \in \Pi$ ,

$$\|\nabla f_t(x)\|_\infty \leq G.$$

A **dynamic comparator** is any sequence  $\{u_t\}_{t=1}^T \subset \Pi$ . Define the per-round path increment

$$\Delta_t := \|u_t - u_{t-1}\|_1 \quad (t \geq 2), \quad \Delta_1 := 0,$$

and the total path length  $P_T := \sum_{t=1}^T \Delta_t$ . The dynamic regret is

$$\text{Reg}_T^{\text{dyn}} := \sum_{t=1}^T (f_t(x_t) - f_t(u_t)),$$

where  $\{x_t\}$  is the algorithm's decision sequence.

### B.1.2. ENTROPY MIRROR DESCENT AND THE ENTROPY COEFFICIENT AS A CONTROL KNOB

The mirror map is the negative entropy

$$\Psi(x) := \sum_{i=1}^K x_i \log x_i,$$

with the Bregman divergence

$$D_\Psi(x, y) := \Psi(x) - \Psi(y) - \langle \nabla \Psi(y), x - y \rangle.$$

Negative entropy is strongly convex w.r.t.  $\ell_1$  on the simplex and  $\Psi$  is bounded on  $\Delta_K$  (scale  $\log K$ ). To avoid  $\nabla \Psi(x)$  diverging on the boundary, the analysis implicitly works on a standard truncated/smoothed domain (e.g.  $x_i \geq \varepsilon$ ) so that the resulting effects are confined to constants/log-factors.

The key modeling component is an entropy-regularized loss

$$\hat{f}_t(x) := f_t(x) + \lambda_t \Psi(x), \quad \lambda_t \geq 0,$$

where  $\lambda_t$  is the scheduled **entropy coefficient**. Heuristically, larger  $\lambda_t$  induces smoother, more randomized decisions (more exploration/robustness), while smaller  $\lambda_t$  approaches greedy exploitation.

### B.1.3. AES-OCO UPDATE RULE

Given nonnegative sequences  $\{\lambda_t\}$  and step sizes  $\{\eta_t\}$ , AES-OCO performs mirror descent on  $\hat{f}_t$ :

$$x_{t+1} = \arg \min_{x \in \Delta_K} \left\{ \eta_t \langle \nabla \hat{f}_t(x_t), x \rangle + D_\Psi(x, x_t) \right\},$$

where

$$\nabla \hat{f}_t(x_t) = \nabla f_t(x_t) + \lambda_t \nabla \Psi(x_t).$$

A core structural choice (formalized below) is the **coupled step size**

$$\eta_t = c \lambda_t, \quad c > 0,$$

which induces the canonical per-round trade-off

$$(\text{tracking cost}) \propto \frac{\text{non-stationarity}}{\lambda_t} \quad + \quad (\text{regularization cost}) \propto \lambda_t.$$

## B.1.4. INTERFACE TO NON-STATIONARY MAXIMUM-ENTROPY RL

The end goal concerns adaptive temperature scheduling in non-stationary RL. The analysis uses the maximum-entropy (soft) formulation so that the soft-optimal policy takes a softmax form, enabling Lipschitz connections between value/advantage variations and policy variations. Conceptually:

1. **OCO layer:** derive a dynamic regret bound for AES-OCO with an explicit per-round trade-off, and provide an online rule for choosing  $\lambda_t$  driven by an observable non-stationarity proxy;
2. **soft-RL layer:** view each state-wise policy update as an entropy-regularized OCO problem; transmit MDP variation to soft- $Q^*$  variation via soft Bellman sensitivity, and then to policy path variation via softmax Lipschitzness;
3. **real RL error accounting:** when moving from full-information planning to sampling and function approximation, explicit bias and occupancy-mismatch terms appear; these are separated as additive error terms and paired with computable non-stationarity estimators to drive  $\lambda_t$  online.

 B.2. From Dynamic Mirror Descent to a  $\lambda$ -Trade-off Bound

A foundational inequality couples mirror descent updates with a dynamic comparator. Let  $\Pi \subset \mathbb{R}^K$  be a closed convex set (e.g., a truncated simplex). Let  $\Psi : \Pi \rightarrow \mathbb{R}$  be differentiable and 1-strongly convex w.r.t. a norm  $\|\cdot\|$ , with dual norm  $\|\cdot\|_*$ . Define the Bregman divergence

$$D_\Psi(x, y) := \Psi(x) - \Psi(y) - \langle \nabla \Psi(y), x - y \rangle. \quad (47)$$

Given vectors  $\{g_t\}$  and step sizes  $\{\eta_t\}$ , mirror descent performs

$$x_{t+1} = \arg \min_{x \in \Pi} \left\{ \eta_t \langle g_t, x \rangle + D_\Psi(x, x_t) \right\}. \quad (48)$$

**Lemma B.1** (Dynamic MD inequality). *Let  $\{u_t\}_{t=1}^T \subset \Pi$  be any comparator sequence and set  $u_0 = u_1$ . Assume bounded mirror gradients: there exists  $G_\Psi < \infty$  such that*

$$\|\nabla \Psi(z)\|_* \leq G_\Psi, \quad \forall z \in \Pi, \quad (49)$$

and assume the step sizes are nondecreasing ( $\eta_t \geq \eta_{t-1}$ ). Then the iterates generated by (3) satisfy

$$\sum_{t=1}^T \langle g_t, x_t - u_t \rangle \leq \frac{D_\Psi(u_1, x_1)}{\eta_1} + \sum_{t=1}^T \frac{\eta_t}{2} \|g_t\|_*^2 + \sum_{t=2}^T \frac{2G_\Psi}{\eta_t} \|u_t - u_{t-1}\|. \quad (50)$$

The inequality in Lemma 3.1 is the central switch: the first two terms match the static-comparator telescoping structure; the last term quantifies the extra cost of comparator drift. A complete proof (with a fully explicit dynamic telescoping argument under the stated conditions) is deferred to Appendix E.

## B.2.1. ENTROPY-REGULARIZED OCO AND DYNAMIC REGRET

Assume convex differentiable  $f_t$  with bounded gradients

$$\|\nabla f_t(x)\|_\infty \leq G, \quad \forall x \in \Pi. \quad (51)$$

Define the regularized loss

$$\hat{f}_t(x) := f_t(x) + \lambda_t \Psi(x). \quad (52)$$

Run mirror descent (3) on  $\hat{f}_t$  with  $g_t = \nabla \hat{f}_t(x_t)$ . By convexity,

$$\hat{f}_t(x_t) - \hat{f}_t(u_t) \leq \langle \nabla \hat{f}_t(x_t), x_t - u_t \rangle. \quad (53)$$

Combining (8) with Lemma 3.1 yields

$$\sum_{t=1}^T (\hat{f}_t(x_t) - \hat{f}_t(u_t)) \leq \frac{D_\Psi(u_1, x_1)}{\eta_1} + \sum_{t=1}^T \frac{\eta_t}{2} \|\nabla \hat{f}_t(x_t)\|_*^2 + \sum_{t=2}^T \frac{2G_\Psi}{\eta_t} \|u_t - u_{t-1}\|. \quad (54)$$

The target is the **unregularized** dynamic regret

$$\text{Reg}_T^{\text{dyn}}(u_{1:T}) := \sum_{t=1}^T (f_t(x_t) - f_t(u_t)). \quad (55)$$

Using  $\hat{\uparrow}_t = f_t + \lambda_t \Psi$  gives the identity

$$f_t(x_t) - f_t(u_t) = (\hat{\uparrow}_t(x_t) - \hat{\uparrow}_t(u_t)) - \lambda_t(\Psi(x_t) - \Psi(u_t)). \quad (56)$$

Since  $|\Psi(x)| \leq \log K$  on the simplex,

$$-\lambda_t(\Psi(x_t) - \Psi(u_t)) \leq 2\lambda_t \log K. \quad (57)$$

Combining (9)–(11) yields the master inequality

$$\text{Reg}_T^{\text{dyn}}(u_{1:T}) \leq \frac{D_\Psi(u_1, x_1)}{\eta_1} + \sum_{t=1}^T \frac{\eta_t}{2} \|\nabla \hat{\uparrow}_t(x_t)\|_*^2 + \sum_{t=2}^T \frac{2G_\Psi}{\eta_t} \|u_t - u_{t-1}\| + 2 \log K \sum_{t=1}^T \lambda_t. \quad (58)$$

### B.2.2. COUPLED STEP SIZES AND THE PER-ROUND TRADE-OFF

**(i) Coupled step size**  $\eta_t = c\lambda_t$ . Choose

$$\eta_t = c\lambda_t, \quad c > 0, \quad (59)$$

and clip  $\lambda_t \in [\lambda_{\min}, \lambda_{\max}]$  with  $\lambda_{\min} > 0$  for numerical stability. Monotonicity of  $\eta_t$  (required by Lemma 3.1) can be ensured by a doubling/epoch construction or by taking a monotone upper envelope.

**(ii) Bounding  $\|\nabla \hat{\uparrow}_t(x_t)\|_\infty$  and reducing higher-order terms.** In the  $\ell_1/\ell_\infty$  pairing,  $\|\cdot\|_* = \|\cdot\|_\infty$ . Since  $\nabla \hat{\uparrow}_t = \nabla f_t + \lambda_t \nabla \Psi$ , by (6) and (4),

$$\|\nabla \hat{\uparrow}_t(x_t)\|_\infty \leq G + \lambda_t G_\Psi. \quad (60)$$

Under a truncated simplex  $\Delta_{K,\varepsilon}$ , negative entropy satisfies

$$G_\Psi = \sup_{x \in \Delta_{K,\varepsilon}} \|\nabla \Psi(x)\|_\infty \leq 1 + |\log \varepsilon|. \quad (61)$$

Substituting (13) and (14) into (12), and absorbing higher-order dependence on  $\lambda_t$  using  $\lambda_t \leq \lambda_{\max}$ , yields the following per-round one-dimensional trade-off.

**Theorem B.2** ( $\lambda$ -trade-off dynamic regret bound). *Run mirror descent (3) on  $\hat{\uparrow}_t$  with the coupled step sizes (13) and  $\lambda_t \in [\lambda_{\min}, \lambda_{\max}]$  (with  $\eta_t$  nondecreasing). Then there exist constants  $C_0, C_1, C_2 > 0$  independent of  $T$  (depending on  $c, G, G_\Psi, \log K, \lambda_{\min}, \lambda_{\max}$ ) such that for any comparator sequence  $u_{1:T} \subset \Pi$ ,*

$$\text{Reg}_T^{\text{dyn}}(u_{1:T}) \leq C_0 + \sum_{t=2}^T \left( C_1 \frac{\alpha_t}{\lambda_t} + C_2 \lambda_t \right), \quad \alpha_t := \|u_t - u_{t-1}\|_1. \quad (62)$$

Equivalently, each round contributes the convex function

$$\varphi_t(\lambda) := C_1 \frac{\alpha_t}{\lambda} + C_2 \lambda, \quad \lambda > 0. \quad (63)$$

The interpretation of (16) is explicit: the first term is the **tracking cost** (larger non-stationarity  $\alpha_t$  favors larger  $\lambda_t$  for faster redistribution of probability mass), while the second term is the **regularization/stability cost** (too large  $\lambda_t$  over-smooths and harms instantaneous optimality).

**Theorem B.3** (Per-round oracle optimal  $\lambda_t$ ). *For each  $t \geq 2$ , define*

$$\lambda_t^* := \arg \min_{\lambda > 0} \varphi_t(\lambda) = \sqrt{\frac{C_1}{C_2} \alpha_t}. \quad (64)$$

Then

$$\text{Reg}_T^{\text{dyn}}(u_{1:T}) \leq C_0 + 2\sqrt{C_1 C_2} \sum_{t=2}^T \sqrt{\alpha_t} \leq C_0 + 2\sqrt{C_1 C_2} \sqrt{T \sum_{t=2}^T \alpha_t}. \quad (65)$$

### B.3. AES-OCO: Fully Online Adaptive Scheduling

This section upgrades the per-round oracle  $\lambda_t^*$  into a fully online schedule driven by an observable non-stationarity proxy. Start from (16) (absorbing constants into  $C_0$  as needed) and rewrite it as

$$\text{Reg}_T^{\text{dyn}} \leq C_0 \log K + \sum_{t=1}^T \left( C_1 \frac{\alpha_t}{\lambda_t} + C_2 \lambda_t \right), \quad \alpha_t := \|u_t - u_{t-1}\|_1. \quad (66)$$

If a constant entropy coefficient  $\lambda_t \equiv \lambda$  is used, then

$$\text{Reg}_T^{\text{dyn}} \leq C_0 \log K + C_1 \frac{A_T}{\lambda} + C_2 T \lambda, \quad A_T := \sum_{t=1}^T \alpha_t, \quad (67)$$

whose minimizer is

$$\lambda^{\text{off}} = \sqrt{\frac{C_1 A_T}{C_2 T}}, \quad \text{Reg}_T^{\text{dyn}} \leq C_0 \log K + 2\sqrt{C_1 C_2 A_T T}. \quad (68)$$

Thus the optimal leading term is  $\sqrt{A_T T}$  once the total non-stationarity  $A_T$  is known.

In general OCO,  $\alpha_t$  is not directly observable. The subsequent soft-RL reduction will upper bound  $\alpha_t$  by an **observable/estimable** non-stationarity signal. The following result is therefore stated with a proxy.

Assume a nonnegative online proxy sequence  $\{\hat{\alpha}_t\}$  such that for all  $t$ ,

$$\alpha_t \leq \hat{\alpha}_t, \quad (69)$$

and define its prefix sum

$$\hat{A}_t := \sum_{s=1}^t \hat{\alpha}_s. \quad (70)$$

Consider the no-restart schedule (before clipping)

$$\lambda_t = \sqrt{\frac{C_1}{C_2}} \sqrt{\frac{\hat{A}_t}{t}}. \quad (71)$$

**Theorem B.4** (Online AES scheduling driven by an observable proxy). *Under the conditions of Theorem 3.2, and assuming the proxy condition (20), choosing  $\lambda_t$  by (22) yields*

$$\text{Reg}_T^{\text{dyn}} \leq C_0 \log K + 4\sqrt{C_1 C_2 T \hat{A}_T}. \quad (72)$$

**Proof.** From (66) and (20),

$$\text{Reg}_T^{\text{dyn}} \leq C_0 \log K + \sum_{t=1}^T \left( C_1 \frac{\hat{\alpha}_t}{\lambda_t} + C_2 \lambda_t \right). \quad (73)$$

Substituting (22) gives

$$\sum_{t=1}^T \left( C_1 \frac{\hat{\alpha}_t}{\lambda_t} + C_2 \lambda_t \right) = \sqrt{C_1 C_2} \sum_{t=1}^T \left( \hat{\alpha}_t \frac{\sqrt{t}}{\sqrt{\hat{A}_t}} + \frac{\sqrt{\hat{A}_t}}{\sqrt{t}} \right). \quad (74)$$

For the first term,  $\sqrt{t} \leq \sqrt{T}$  implies

$$\sum_{t=1}^T \hat{\alpha}_t \frac{\sqrt{t}}{\sqrt{\hat{A}_t}} \leq \sqrt{T} \sum_{t=1}^T \frac{\hat{\alpha}_t}{\sqrt{\hat{A}_t}}. \quad (75)$$

The standard inequality (proved in Appendix I) gives

$$\sum_{t=1}^T \frac{\hat{\alpha}_t}{\sqrt{\hat{A}_t}} \leq 2\sqrt{\hat{A}_T}, \quad (76)$$

so the first term is  $\leq 2\sqrt{T\hat{A}_T}$ . For the second term, Appendix I also yields

$$\sum_{t=1}^T \frac{\sqrt{\hat{A}_t}}{\sqrt{t}} \leq 2\sqrt{T\hat{A}_T}. \quad (77)$$

Plugging (75)–(77) into (74) and then into (73) yields (23).  $\square$

**Clipped implementation.** In practice,  $\lambda_t$  is clipped for stability:

$$\lambda_t = \text{clip}_{[\lambda_{\min}, \lambda_{\max}]} \left( \sqrt{\frac{C_1}{C_2}} \sqrt{\frac{\hat{A}_t}{t}} \right). \quad (78)$$

Clipping introduces only lower-order additive compensation terms (e.g., when  $\lambda_t = \lambda_{\max}$ , the contribution  $\sum \hat{\alpha}_t / \lambda_{\max}$  is bounded), formalized in Appendix J.

#### B.4. AES-RL: Reduction for Non-stationary Soft RL

Consider a sequence of non-stationary discounted MDPs  $\{M_t\}_{t=1}^T$  with

$$M_t = (\mathcal{S}, \mathcal{A}, P_t, r_t, \rho, \gamma), \quad \gamma \in (0, 1),$$

and bounded rewards  $|r_t(s, a)| \leq 1$ . For any policy  $\pi$ , define the maximum-entropy (soft) return at time  $t$ :

$$J_t(\pi) := \mathbb{E} \left[ \sum_{h=0}^{\infty} \gamma^h (r_t(s_h, a_h) + \mu H(\pi(\cdot | s_h))) \mid s_0 \sim \rho, a_h \sim \pi(\cdot | s_h), s_{h+1} \sim P_t(\cdot | s_h, a_h) \right],$$

where  $\mu > 0$  is a fixed baseline temperature and  $\pi_t^* \in \arg \max_{\pi} J_t(\pi)$  is the soft-optimal policy at round  $t$ . Define the RL dynamic regret

$$\text{Reg}_T^{\text{RL}} := \sum_{t=1}^T (J_t(\pi_t^*) - J_t(\pi_t)).$$

##### B.4.1. FROM SOFT-RL TO AN ENTROPY-REGULARIZED OCO SURROGATE

Let  $Q_t^*$  denote the soft-optimal  $Q$ -function of  $M_t$  (satisfying the soft Bellman optimality equation). For each state  $s$ , define the local linear-entropy loss over the simplex  $\Delta(\mathcal{A})$ :

$$f_{t,s}(\pi_s) := -\langle Q_t^*(s, \cdot), \pi_s \rangle + \mu \Psi(\pi_s), \quad \Psi(p) := \sum_a p(a) \log p(a) = -H(p).$$

View the policy as a product variable  $\pi = (\pi(\cdot | s))_{s \in \mathcal{S}} \in \prod_s \Delta(\mathcal{A})$  and define the separable mirror potential

$$\Psi_{\text{tot}}(\pi) := \sum_{s \in \mathcal{S}} \Psi(\pi(\cdot | s)).$$

Let  $d_t^*$  be the (normalized) discounted occupancy measure of  $\pi_t^*$  under  $M_t$ :

$$d_t^*(s) := (1 - \gamma) \sum_{h \geq 0} \gamma^h \Pr_{M_t, \pi_t^*}(s_h = s), \quad \sum_s d_t^*(s) = 1.$$

Define the per-round surrogate loss

$$F_t(\pi) := \sum_{s \in \mathcal{S}} d_t^*(s) f_{t,s}(\pi(\cdot | s)).$$

A standard soft performance-difference decomposition (formalized in the appendix) yields that

$$J_t(\pi_t^*) - J_t(\pi_t) \leq \frac{C_J}{1 - \gamma} (F_t(\pi_t) - F_t(\pi_t^*)) + \text{Bias}_t,$$

where  $C_J$  is a constant depending only on reward/entropy bounds, and  $\text{Bias}_t$  collects the interface residuals (zero in an ideal planning/full-information setting; explicit in sampling/function approximation).

AES is applied by running mirror descent on

$$\mathcal{L}_t(\pi) := F_t(\pi) + \lambda_t \Psi_{\text{tot}}(\pi),$$

with  $\eta_t = c\lambda_t$  and the online schedule from Theorem 3.4 driven by an RL-specific observable proxy  $\widehat{\alpha}_t$ .

#### B.4.2. KEY BRIDGE: MDP VARIATION $\Rightarrow$ PATH VARIATION OF $\pi_t^*$

Define the non-stationarity budget (reward + transition)

$$B_T^{\text{MDP}} := \sum_{t=2}^T \left( \Delta_t^r + \gamma V_{\max} \Delta_t^P \right),$$

where

$$\Delta_t^r := \sup_{s,a} |r_t(s,a) - r_{t-1}(s,a)|, \quad \Delta_t^P := \sup_{s,a} \text{TV}(P_t(\cdot|s,a), P_{t-1}(\cdot|s,a)),$$

and  $V_{\max} \geq \sup_{t,s} |V_t^*(s)|$  (for bounded rewards,  $V_{\max} = O((1 + \mu \log |\mathcal{A}|)/(1 - \gamma))$ ).

**(i) Soft Bellman sensitivity.** Let  $\mathcal{T}_t$  be the soft Bellman optimality operator of  $M_t$ ; it is a  $\gamma$ -contraction. The standard fixed-point perturbation bound gives

$$\|Q_t^* - Q_{t-1}^*\|_\infty \leq \frac{1}{1 - \gamma} \left( \Delta_t^r + \gamma V_{\max} \Delta_t^P \right). \quad (79)$$

**(ii) Softmax Lipschitzness.** For each state  $s$ , the soft-optimal policy satisfies

$$\pi_t^*(\cdot|s) = \text{softmax}(Q_t^*(s, \cdot)/\mu).$$

Using the  $\ell_1$ - $\ell_\infty$  Lipschitz property of softmax (proved in the appendix),

$$\|\pi_t^*(\cdot|s) - \pi_{t-1}^*(\cdot|s)\|_1 \leq \frac{1}{\mu} \|Q_t^* - Q_{t-1}^*\|_\infty. \quad (80)$$

Define the local path increment

$$\alpha_{t,s} := \|\pi_t^*(\cdot|s) - \pi_{t-1}^*(\cdot|s)\|_1.$$

Combining (25) and (26) yields

$$\sum_{t=2}^T \sum_{s \in \mathcal{S}} \alpha_{t,s} \leq \frac{|\mathcal{S}|}{\mu(1 - \gamma)} B_T^{\text{MDP}}.$$

Consequently, one may drive the OCO proxy by a quantity proportional to the (estimated) drift magnitude of soft- $Q^*$  (or a stable surrogate such as critic drift in function approximation).

#### B.4.3. OVERALL RESULT: PLANNING-VERSION BOUND (PRINCIPAL TERM)

**Theorem B.5** (AES-RL-Plan: non-stationary soft-RL dynamic regret (principal term)). *In the non-stationary tabular soft-MDP sequence above with bounded rewards, run AES with the per-round surrogate losses  $f_{t,s}(\pi_s) = -\langle Q_t^*(s, \cdot), \pi_s \rangle + \mu \Psi(\pi_s)$  and an online schedule  $\{\lambda_t\}$  driven by a valid non-stationarity proxy (Theorem 3.4). Then there exists a constant  $C$  such that*

$$\text{Reg}_T^{\text{RL}} \leq \widetilde{O} \left( \frac{\sqrt{|\mathcal{S}| \log |\mathcal{A}|}}{\mu(1 - \gamma)^2} \sqrt{B_T^{\text{MDP}} T} \right) + \sum_{t=1}^T \text{Bias}_t,$$

where  $\widetilde{O}(\cdot)$  hides logarithmic factors in  $T, |\mathcal{S}|$ , and  $\text{Bias}_t$  collects the planning-to-RL interface residuals.

**Corresponding appendices.** The soft Bellman sensitivity and the softmax Lipschitz lemma are provided in the appendices. The equalities-level performance-difference decomposition and the explicit form/control of  $\text{Bias}_t$  are deferred to the appendix material.

### B.5. From Planning to Real RL: Explicit Error Decomposition

The previous subsection emphasizes the principal non-stationarity term and assumes ideal objects (e.g.  $Q_t^*$  and  $d_t^{\pi^*}$ ). In real RL (especially off-policy learning with function approximation), two traceable deviations arise: **(i)** a  $Q^*$ -substitution bias and **(ii)** an occupancy-weight mismatch error. A clean inequality separates the principal term and these errors; formal proofs and control strategies are deferred to the appendix.

Let

$$f_{t,s}(\pi_s) := -\langle Q_t^*(s, \cdot), \pi_s \rangle + \mu \Psi(\pi_s), \quad \Delta_{t,s} := f_{t,s}(\pi_t(\cdot | s)) - f_{t,s}(\pi_t^*(\cdot | s)).$$

For any state-weighting distribution  $\tilde{d}_t$  used by the algorithm (e.g. on-policy  $d_t^{\pi^*}$  or a replay-buffer empirical distribution), there exist error terms  $\text{bias}_t$  and  $\text{occ}_t(\tilde{d}_t)$  such that for each  $t$ ,

$$J_t(\pi_t^*) - J_t(\pi_t) \leq \frac{1}{1-\gamma} \mathbb{E}_{s \sim \tilde{d}_t} [\Delta_{t,s}] + \text{bias}_t + \frac{1}{1-\gamma} \text{occ}_t(\tilde{d}_t). \quad (81)$$

Here  $\text{bias}_t$  arises from substituting  $Q_t^*$  for  $Q_t^{\pi^*}$  (and from estimator errors when  $Q$  is approximated), while  $\text{occ}_t(\tilde{d}_t)$  arises from substituting  $\tilde{d}_t$  for  $d_t^{\pi^*}$ . The main results keep  $\sum_t \text{bias}_t$  and  $\sum_t \text{occ}_t(\tilde{d}_t)$  explicitly as additive terms; in algorithm instantiation and experiments they correspond to function-approximation error and off-policy distribution shift, which can be reduced by stabilization techniques (slow targets, conservative updates, reweighting, etc.).

## C. Equivalent Forms of the AES–OCO Update

### C.1. Primal and dual forms for negative-entropy mirror descent

Consider mirror descent on  $\Pi = \Delta_K$  with mirror map  $\Psi$  and step size  $\eta_t > 0$ :

$$x_{t+1} = \arg \min_{x \in \Delta_K} \{\eta_t \langle g_t, x \rangle + D_\Psi(x, x_t)\}. \quad (82)$$

For  $\Psi(x) = \sum_i x_i \log x_i$ , (B.1) is equivalent to an exponentiated-gradient update. Writing the dual variable as  $y_t := \nabla \Psi(x_t)$ , the optimality condition implies

$$\nabla \Psi(x_{t+1}) = \nabla \Psi(x_t) - \eta_t g_t + \nu_t \mathbf{1}, \quad (83)$$

where  $\nu_t$  enforces the simplex constraint. Exponentiating coordinatewise yields

$$x_{t+1,i} \propto x_{t,i} \exp(-\eta_t g_{t,i}), \quad i \in [K], \quad (84)$$

followed by normalization. Thus AES–OCO can be implemented either via the primal proximal form (B.1) or the multiplicative weights form (B.3).

**Notation remark (entropy coefficient vs. inverse temperature).** In the multiplicative form, the scalar step size  $\eta_t$  acts as an inverse temperature in the sense that, for a one-step update with  $g_t = -r_t$  and a uniform  $x_t$ , the resulting  $x_{t+1}$  has a softmax form with temperature proportional to  $1/\eta_t$ . To avoid symbol confusion in the experiments, we denote the scheduled inverse-temperature knob by  $\beta_t$  and report the corresponding entropy coefficient in the regularized objective via  $\lambda_t := 1/\beta_t$ .

### C.2. Why coupling $\eta_t = c\lambda_t$ produces a one-knob trade-off

The core regret bound in the paper contains, per round, two antagonistic contributions: a **tracking term** scaling like  $\alpha_t/\eta_t$  (from dynamic comparators), and a **stability/regularization term** scaling like  $\eta_t$  (from gradient control). When the per-round objective is

$$\ell_t(x) = f_t(x) + \lambda_t \Psi(x), \quad (85)$$

a natural design is to couple the mirror step size with the entropy weight:

$$\eta_t = c\lambda_t, \quad c > 0. \quad (86)$$

Under this coupling, the tracking part becomes proportional to  $\alpha_t/\lambda_t$ , while the stability part becomes proportional to  $\lambda_t$ . This yields a per-round scalar trade-off of the form

$$C_1 \frac{\alpha_t}{\lambda_t} + C_2 \lambda_t, \quad (87)$$

which can be optimized either offline (Appendix H) or online via adaptive schedules (Appendix I and Appendix J).

## D. Preparations: A Robust Dynamic Mirror-Descent Inequality

### D.1. One-step mirror descent inequality (static comparator)

Let  $\Pi \subseteq \mathbb{R}^d$  be closed and convex. Fix a norm  $|\cdot|$  with dual norm  $|\cdot|_*$ . Assume  $\Psi : \Pi \rightarrow \mathbb{R}$  is differentiable and 1-strongly convex w.r.t.  $|\cdot|$ , i.e.,

$$\Psi(x) \geq \Psi(y) + \langle \nabla \Psi(y), x - y \rangle + \frac{1}{2}|x - y|^2, \quad \forall x, y \in \Pi. \quad (88)$$

Define  $D_\Psi$  as usual. Consider one mirror descent step:

$$x_{t+1} = \arg \min_{x \in \Pi} \{\eta_t \langle g_t, x \rangle + D_\Psi(x, x_t)\}, \quad \eta_t > 0. \quad (89)$$

**Lemma D.1** (One-step MD inequality (static comparator)). *For any fixed  $u \in \Pi$ , the update (C.1) satisfies*

$$\langle g_t, x_t - u \rangle \leq \frac{D_\Psi(u, x_t) - D_\Psi(u, x_{t+1})}{\eta_t} + \frac{\eta_t}{2} |g_t|_*^2. \quad (90)$$

*Proof.* First-order optimality of (C.1) implies that for any  $x \in \Pi$ ,

$$\langle \eta_t g_t + \nabla \Psi(x_{t+1}) - \nabla \Psi(x_t), x - x_{t+1} \rangle \geq 0. \quad (91)$$

Setting  $x = u$  yields

$$\eta_t \langle g_t, x_{t+1} - u \rangle \leq \langle \nabla \Psi(x_{t+1}) - \nabla \Psi(x_t), u - x_{t+1} \rangle. \quad (92)$$

Apply the three-point identity (Appendix A.2) with  $(a, b, c) = (u, x_{t+1}, x_t)$ :

$$\langle \nabla \Psi(x_{t+1}) - \nabla \Psi(x_t), u - x_{t+1} \rangle D_\Psi(u, x_t) - D_\Psi(u, x_{t+1}) - D_\Psi(x_{t+1}, x_t). \quad (93)$$

Combine (C.4) and (C.5):

$$\eta_t \langle g_t, x_{t+1} - u \rangle \leq D_\Psi(u, x_t) - D_\Psi(u, x_{t+1}) - D_\Psi(x_{t+1}, x_t). \quad (94)$$

Now decompose

$$\langle g_t, x_t - u \rangle \langle g_t, x_t - x_{t+1} \rangle + \langle g_t, x_{t+1} - u \rangle, \quad (95)$$

multiply by  $\eta_t$ , and use (C.6):

$$\eta_t \langle g_t, x_t - u \rangle \leq \eta_t \langle g_t, x_t - x_{t+1} \rangle D_\Psi(u, x_t) - D_\Psi(u, x_{t+1}) - D_\Psi(x_{t+1}, x_t). \quad (96)$$

By Hölder and Young,

$$\eta_t \langle g_t, x_t - x_{t+1} \rangle \leq \eta_t |g_t|_* |x_t - x_{t+1}| \leq \frac{\eta_t^2}{2} |g_t|_*^2 + \frac{1}{2} |x_t - x_{t+1}|^2. \quad (97)$$

Strong convexity implies  $D_\Psi(x_{t+1}, x_t) \geq \frac{1}{2}|x_{t+1} - x_t|^2$ , so the last two terms in (C.8) are non-positive after inserting (C.9) and can be dropped. Dividing by  $\eta_t$  gives (C.2).  $\square$

## D.2. Telescoping with dynamic comparators and the drift term

Let  $u_{t=1}^T \subseteq \Pi$  be an arbitrary comparator sequence. Apply Lemma D.1 with  $u = u_t$  and sum over  $t$ :

$$\sum_{t=1}^T \langle g_t, x_t - u_t \rangle \leq \sum_{t=1}^T \frac{D_\Psi(u_t, x_t) - D_\Psi(u_t, x_{t+1})}{\eta_t} + \sum_{t=1}^T \frac{\eta_t}{2} |g_t|_*^2. \quad (98)$$

The first sum is not a perfect telescope because  $u_t$  changes with  $t$ . The following exact algebraic decomposition identifies all residuals:

$$\begin{aligned} \sum_{t=1}^T \frac{D_\Psi(u_t, x_t) - D_\Psi(u_t, x_{t+1})}{\eta_t} = \\ \frac{D_\Psi(u_1, x_1)}{\eta_1} + \sum_{t=2}^T D_\Psi(u_t, x_t) \left( \frac{1}{\eta_t} - \frac{1}{\eta_{t-1}} \right) + \sum_{t=2}^T \frac{D_\Psi(u_t, x_t) - D_\Psi(u_{t-1}, x_t)}{\eta_{t-1}} - \frac{D_\Psi(u_T, x_{T+1})}{\eta_T}. \end{aligned} \quad (99)$$

This is obtained by re-indexing the second term and adding/subtracting  $D_\Psi(u_{t-1}, x_t)$  inside the bracket; no inequality is used.

**Step-size monotonicity removes the step-size-change residual.** If  $\eta_t$  is nondecreasing (equivalently  $1/\eta_t$  is nonincreasing), then

$$\frac{1}{\eta_t} - \frac{1}{\eta_{t-1}} \leq 0, \quad (100)$$

and since  $D_\Psi \geq 0$ , the second term in (C.11) is non-positive and can be dropped. This is the sole reason to enforce nondecreasing  $\eta_t$ , typically via doubling/epoch constructions.

**A clean drift control under bounded mirror gradients.** To control the comparator-change residual, assume:

**Assumption D.2** (Bounded mirror gradient). There exists  $G_\Psi < \infty$  such that  $|\nabla \Psi(x)|_* \leq G_\Psi$  for all  $x \in \Pi$ .

Under Assumption D.2,

$$D_\Psi(u_t, x) - D_\Psi(u_{t-1}, x) \Psi(u_t) - \Psi(u_{t-1}) - \langle \nabla \Psi(x), u_t - u_{t-1} \rangle \leq \langle \nabla \Psi(u_t) - \nabla \Psi(x), u_t - u_{t-1} \rangle, \quad (101)$$

and therefore, by convexity of  $\Psi$  and Hölder,

$$D_\Psi(u_t, x) - D_\Psi(u_{t-1}, x) \leq |\nabla \Psi(x)|_*, |u_t - u_{t-1}| \leq G_\Psi |u_t - u_{t-1}|. \quad (102)$$

For the negative entropy on  $\Delta_{K,\varepsilon}$  with  $|\cdot| = |\cdot|_1$  and  $|\cdot|_* = |\cdot|_\infty$ , Appendix F gives  $G_\Psi \leq 1 + |\log \varepsilon|$ .

## D.3. Summed dynamic inequality (robust form)

Combining (C.10)–(C.12), dropping non-positive terms (including  $D_\Psi(u_T, x_{T+1})/\eta_T$ ), and specializing to  $|\cdot| = |\cdot|_1$  gives:

$$\sum_{t=1}^T \langle g_t, x_t - u_t \rangle \leq \frac{D_\Psi(u_1, x_1)}{\eta_1} + \sum_{t=1}^T \frac{\eta_t}{2} |g_t|_\infty^2 + \sum_{t=2}^T \frac{G_\Psi}{\eta_{t-1}} |u_t - u_{t-1}|_1, \quad (103)$$

provided  $\eta_t$  is nondecreasing and Assumption D.2 holds.

## E. Complete Proof of Lemma 3.1 (Dynamic Comparator Handling)

This appendix presents the specialized proof of Lemma 3.1 used in the main text, following a fully explicit algebraic decomposition and relying only on two minimal conditions: (i) nondecreasing step sizes  $\eta_t$  (equivalently nonincreasing  $1/\eta_t$ ); and (ii) bounded mirror gradients  $|\nabla \Psi(x)|_\infty \leq G_\Psi$  on the feasible set.

### E.1. Static one-step inequality

Consider the mirror descent update (main text Eq. (3)):

$$x_{t+1} = \arg \min_{x \in \Pi} \{\eta_t \langle g_t, x \rangle + D_\Psi(x, x_t)\}, \quad (104)$$

where  $\Pi$  is closed and convex,  $\Psi$  is differentiable and 1-strongly convex w.r.t.  $|\cdot|_1$ , and the dual norm is  $|\cdot|_\infty$ .

**Lemma E.1** (Static MD inequality). *For any fixed  $u \in \Pi$ , the iterate pair  $(x_t, x_{t+1})$  generated by (D.1) satisfies*

$$\langle g_t, x_t - u \rangle \leq \frac{D_\Psi(u, x_t) - D_\Psi(u, x_{t+1})}{\eta_t} + \frac{\eta_t}{2} |g_t|_\infty^2. \quad (105)$$

*Proof.* This is Lemma D.1 instantiated with  $|\cdot| = |\cdot|_1$  and  $|\cdot|_* = |\cdot|_\infty$ .  $\square$

### E.2. Summation with dynamic comparators: exact decomposition

Let  $u_{t=1}^T \subseteq \Pi$  be any comparator sequence. Apply Lemma E.1 with  $u = u_t$  and sum:

$$\sum_{t=1}^T \langle g_t, x_t - u_t \rangle \leq \sum_{t=1}^T \frac{D_\Psi(u_t, x_t) - D_\Psi(u_t, x_{t+1})}{\eta_t} + \sum_{t=1}^T \frac{\eta_t}{2} |g_t|_\infty^2. \quad (106)$$

Define

$$S := \sum_{t=1}^T \frac{D_\Psi(u_t, x_t) - D_\Psi(u_t, x_{t+1})}{\eta_t}. \quad (107)$$

Write  $S$  as a difference of two sums and re-index the second:

$$S = \sum_{t=1}^T \frac{D_\Psi(u_t, x_t)}{\eta_t} - \sum_{t=1}^T \frac{D_\Psi(u_t, x_{t+1})}{\eta_t} = \frac{D_\Psi(u_1, x_1)}{\eta_1} + \sum_{t=2}^T \frac{D_\Psi(u_t, x_t)}{\eta_t} - \sum_{t=2}^T \frac{D_\Psi(u_{t-1}, x_t)}{\eta_{t-1}} - \frac{D_\Psi(u_T, x_{T+1})}{\eta_T}.$$

Insert and subtract  $\frac{D_\Psi(u_t, x_t)}{\eta_{t-1}}$  inside the middle bracket:

$$\sum_{t=2}^T \frac{D_\Psi(u_t, x_t)}{\eta_t} - \sum_{t=2}^T \frac{D_\Psi(u_{t-1}, x_t)}{\eta_{t-1}} = \sum_{t=2}^T D_\Psi(u_t, x_t) \left( \frac{1}{\eta_t} - \frac{1}{\eta_{t-1}} \right) + \sum_{t=2}^T \frac{D_\Psi(u_t, x_t) - D_\Psi(u_{t-1}, x_t)}{\eta_{t-1}}.$$

Up to this point, all steps are identities.

### E.3. Controlling residuals under minimal assumptions

**Step-size monotonicity eliminates the step-size-change term.** If  $\eta_t$  is nondecreasing, then  $(1/\eta_t - 1/\eta_{t-1}) \leq 0$ , and since  $D_\Psi \geq 0$ ,

$$\sum_{t=2}^T D_\Psi(u_t, x_t) \left( \frac{1}{\eta_t} - \frac{1}{\eta_{t-1}} \right) \leq 0. \quad (108)$$

Hence it can be dropped in an upper bound.

**Bounding the comparator-drift term by a path variation.** For any fixed  $x \in \Pi$ ,

$$\begin{aligned} D_\Psi(u_t, x) - D_\Psi(u_{t-1}, x) &= \Psi(u_t) - \Psi(u_{t-1}) - \langle \nabla \Psi(x), u_t - u_{t-1} \rangle \\ &\leq \langle \nabla \Psi(u_t) - \nabla \Psi(x), u_t - u_{t-1} \rangle \leq |\nabla \Psi(x)|_\infty, |u_t - u_{t-1}|_1. \end{aligned} \quad (109)$$

Assuming  $|\nabla \Psi(x)|_\infty \leq G_\Psi$  for all  $x \in \Pi$  (guaranteed by truncation; Appendix F), it follows that

$$D_\Psi(u_t, x) - D_\Psi(u_{t-1}, x) \leq G_\Psi |u_t - u_{t-1}|_1. \quad (110)$$

#### E.4. Conclusion: Lemma 3.1

Combining (D.3)–(D.8), dropping the non-positive term (D.6) and the terminal nonnegative term  $D_\Psi(u_T, x_{T+1})/\eta_T$ , yields

$$\sum_{t=1}^T \langle g_t, x_t - u_t \rangle \leq \frac{D_\Psi(u_1, x_1)}{\eta_1} + \sum_{t=1}^T \frac{\eta_t}{2} |g_t|_\infty^2 + \sum_{t=2}^T \frac{G_\Psi}{\eta_{t-1}} |u_t - u_{t-1}|_1, \quad (111)$$

which is the stated dynamic-comparator mirror-descent inequality used as Lemma 3.1 in the main text.

## F. Negative Entropy on the Truncated Simplex: Boundedness and Gradient Bounds

This appendix records two basic facts used to track constants: (i)  $|\Psi(x)| \leq \log K$  on  $\Delta_K$ ; and (ii)  $|\nabla \Psi(x)|_\infty \leq 1 + |\log \varepsilon|$  on  $\Delta_{K,\varepsilon}$ .

### F.1. Boundedness: $|\Psi(x)| \leq \log K$

Recall  $\Psi(x) = \sum_{i=1}^K x_i \log x_i$  on  $\Delta_K$ .

**Proposition F.1.** *For any  $x \in \Delta_K$ ,*

$$-\log K \leq \Psi(x) \leq 0, \quad \text{hence} \quad |\Psi(x)| \leq \log K. \quad (112)$$

*Proof.* Since  $x_i \in [0, 1]$ ,  $\log x_i \leq 0$  and thus  $x_i \log x_i \leq 0$ , giving  $\Psi(x) \leq 0$ . For the lower bound,  $\phi(z) = z \log z$  is convex on  $z > 0$ . Under  $\sum_i x_i = 1$ , Jensen (or KKT) shows the minimum is attained at  $x_i = 1/K$ , giving  $\Psi(1/K) = -\log K$ .  $\square$

A direct corollary used in the main text is: for any  $\lambda \geq 0$  and  $x, u \in \Delta_K$ ,

$$-\lambda(\Psi(x) - \Psi(u)) \leq \lambda|\Psi(x)| + \lambda|\Psi(u)| \leq 2\lambda \log K. \quad (113)$$

### F.2. Gradient bound on $\Delta_{K,\varepsilon}$

Consider  $\Delta_{K,\varepsilon} = x \in \Delta_K : x_i \geq \varepsilon, \forall i$  with  $\varepsilon \in (0, 1/K]$ . For  $x \in \Delta_{K,\varepsilon}$ ,

$$\frac{\partial \Psi(x)}{\partial x_i} = 1 + \log x_i. \quad (114)$$

**Proposition F.2** (Gradient  $\ell_\infty$  bound). *For any  $x \in \Delta_{K,\varepsilon}$ ,*

$$|\nabla \Psi(x)|_\infty = \max_{i \in [K]} |1 + \log x_i| \leq 1 + |\log \varepsilon|. \quad (115)$$

*Proof.* Since  $x_i \geq \varepsilon$ ,  $\log x_i \geq \log \varepsilon$ ; since  $x_i \leq 1$ ,  $\log x_i \leq 0$ . Hence  $|\log x_i| \leq |\log \varepsilon|$  and therefore  $|1 + \log x_i| \leq 1 + |\log \varepsilon|$  for all  $i$ .  $\square$

Define

$$G_\Psi := \sup_{x \in \Delta_{K,\varepsilon}} |\nabla \Psi(x)|_\infty \leq 1 + |\log \varepsilon|. \quad (116)$$

Choosing  $\varepsilon = T^{-c}$  implies  $|\log \varepsilon| = O(\log T)$ , so truncation affects only logarithmic factors.

## G. Tracking constants for Theorem 3.2

This appendix reorganizes the intermediate bound (main text Eq. (12)) into the per-round trade-off form (main text Eq. (16)), and makes the constants  $C_0, C_1, C_2$  explicit.

### G.1. Starting point

Recall the intermediate bound: for any comparator sequence  $u_{1:T} \subset \Pi$ ,

$$\text{Reg}_T^{\text{dyn}}(u_{1:T}) \leq \frac{D_\Psi(u_1, x_1)}{\eta_1} + \sum_{t=1}^T \frac{\eta_t}{2} |\nabla \ell_t(x_t)|_\infty^2 + \sum_{t=2}^T \frac{2G_\Psi}{\eta_t} |u_t - u_{t-1}|_1 + 2 \log K \sum_{t=1}^T \lambda_t, \quad (117)$$

where  $\ell_t(x) = f_t(x) + \lambda_t \Psi(x)$ , and  $|\nabla f_t(x)|_\infty \leq G$ .

The target form is

$$\text{Reg}_T^{\text{dyn}}(u_{1:T}) \leq C_0 + \sum_{t=2}^T \left( C_1 \frac{\alpha_t}{\lambda_t} + C_2 \lambda_t \right), \quad \alpha_t := |u_t - u_{t-1}|_1. \quad (118)$$

### G.2. Coupling $\eta_t = c\lambda_t$ yields $\alpha_t/\lambda_t$

Let

$$\eta_t = c\lambda_t, \quad c > 0. \quad (119)$$

Then the drift term in (F.1) becomes

$$\sum_{t=2}^T \frac{2G_\Psi}{\eta_t} |u_t - u_{t-1}|_1 \sum_{t=2}^T \frac{2G_\Psi}{c} \frac{\alpha_t}{\lambda_t}, \quad (120)$$

so one may take

$$C_1 := \frac{2G_\Psi}{c}. \quad (121)$$

### G.3. Linearizing the gradient term via clipping

Since  $\nabla \ell_t = \nabla f_t + \lambda_t \nabla \Psi$ , the triangle inequality gives

$$|\nabla \ell_t(x_t)|_\infty \leq |\nabla f_t(x_t)|_\infty + \lambda_t |\nabla \Psi(x_t)|_\infty \leq G + \lambda_t G_\Psi. \quad (122)$$

Substitute (F.6) into (F.1) and use (F.3):

$$\sum_{t=1}^T \frac{\eta_t}{2} |\nabla \ell_t(x_t)|_\infty^2 \leq \sum_{t=1}^T \frac{c\lambda_t}{2} (G + \lambda_t G_\Psi)^2. \quad (123)$$

Assume a standard upper clipping:

$$0 < \lambda_t \leq \lambda_{\max}, \quad \forall t. \quad (124)$$

Then for all  $t$ ,

$$(G + \lambda_t G_\Psi)^2 \leq (G + \lambda_{\max} G_\Psi)^2 =: M^2. \quad (125)$$

Therefore,

$$\sum_{t=1}^T \frac{\eta_t}{2} |\nabla \ell_t(x_t)|_\infty^2 \leq \sum_{t=1}^T \frac{c\lambda_t}{2} M^2 \frac{cM^2}{2} \sum_{t=1}^T \lambda_t. \quad (126)$$

### G.4. Initial term and a lower clipping $\lambda_{\min}$

The initial term in (F.1) is  $D_\Psi(u_1, x_1)/\eta_1$ . For negative entropy, if  $x_1 = \mathbf{1}/K$ , then for any  $u_1 \in \Delta_K$ ,

$$D_\Psi(u_1, x_1) = \text{KL}(u_1 \mid \mathbf{1}/K) \leq \log K. \quad (127)$$

If a lower clipping is also enforced,

$$\lambda_t \geq \lambda_{\min} > 0, \quad \forall t, \quad (128)$$

then  $\eta_1 = c\lambda_1 \geq c\lambda_{\min}$  and hence

$$\frac{D_\Psi(u_1, x_1)}{\eta_1} \leq \frac{\log K}{c\lambda_{\min}}. \quad (129)$$

### G.5. Final constants

Combine (F.4), (F.10), and the entropy compensation term  $2 \log K \sum_{t=1}^T \lambda_t$  in (F.1), and use (F.13) for the initial term:

$$\text{Reg}_T^{\text{dyn}}(u_{1:T}) \leq \underbrace{\frac{\log K}{c\lambda_{\min}}}_{=:C_0} + \sum_{t=2}^T \underbrace{\frac{2G_{\Psi}}{c} \frac{\alpha_t}{\lambda_t}}_{=:C_1} + \underbrace{\left( \frac{c}{2}(G + \lambda_{\max}G_{\Psi})^2 + 2 \log K \right)}_{=:C_2} \sum_{t=1}^T \lambda_t. \quad (130)$$

Absorbing the  $t = 1$  term of  $\sum_{t=1}^T \lambda_t$  into  $C_0$  yields the desired per-round form (F.2). In particular, a concrete choice is:

$$\boxed{C_1 = \frac{2G_{\Psi}}{c}, \quad C_2 = \frac{c}{2}(G + \lambda_{\max}G_{\Psi})^2 + 2 \log K, \quad C_0 = \frac{\log K}{c\lambda_{\min}} + C_2\lambda_1.} \quad (131)$$

For negative entropy on  $\Delta_{K,\varepsilon}$ , Appendix F gives  $G_{\Psi} \leq 1 + |\log \varepsilon|$ .

## H. Optimal offline constant choice of $\lambda$

Starting from the trade-off bound

$$\text{Reg}_T^{\text{dyn}}(u_{1:T}) \leq C_0 + \sum_{t=2}^T \left( C_1 \frac{\alpha_t}{\lambda_t} + C_2 \lambda_t \right), \quad \alpha_t := |u_t - u_{t-1}|_1, \quad (132)$$

this appendix derives the best offline constant choice  $\lambda_t \equiv \lambda$ , proves the offline constant minimizer (Section 3), and relates it to the per-round oracle minimizer.

### H.1. Reduction under $\lambda_t \equiv \lambda$

If  $\lambda_t \equiv \lambda$ ,

$$\sum_{t=2}^T \frac{\alpha_t}{\lambda_t} \frac{1}{\lambda} \sum_{t=2}^T \alpha_t \frac{A_T}{\lambda}, \quad \sum_{t=2}^T \lambda_t = (T-1)\lambda, \quad (133)$$

where  $A_T := \sum_{t=2}^T \alpha_t$ . Plugging into (G.1) yields

$$\text{Reg}_T^{\text{dyn}}(u_{1:T}) \leq C_0 + C_1 \frac{A_T}{\lambda} + C_2(T-1)\lambda \lesssim C_0 + C_1 \frac{A_T}{\lambda} + C_2 T \lambda. \quad (134)$$

### H.2. One-dimensional minimization and (3.3)

Consider  $\phi(\lambda) = C_1 A_T / \lambda + C_2 T \lambda$  for  $\lambda > 0$ . Then

$$\phi'(\lambda) = -C_1 \frac{A_T}{\lambda^2} + C_2 T, \quad (135)$$

so the minimizer is

$$\lambda^{\text{off}} = \sqrt{\frac{C_1}{C_2} \cdot \frac{A_T}{T}}. \quad (136)$$

Substituting gives

$$\phi(\lambda^{\text{off}}) = 2\sqrt{C_1 C_2 A_T T}, \quad (137)$$

and therefore

$$\text{Reg}_T^{\text{dyn}}(u_{1:T}) \leq C_0 + 2\sqrt{C_1 C_2 A_T T}. \quad (138)$$

### H.3. Relation to the per-round oracle (Theorem 3.3)

The per-round oracle minimizes  $C_1\alpha_t/\lambda + C_2\lambda$  and yields

$$\lambda_t^* = \sqrt{\frac{C_1}{C_2}\alpha_t}. \quad (139)$$

Its induced bound scales with  $\sum_t \sqrt{\alpha_t}$ , and Cauchy–Schwarz implies

$$\sum_{t=2}^T \sqrt{\alpha_t} \leq \sqrt{(T-1) \sum_{t=2}^T \alpha_t} \lesssim \sqrt{A_T T}. \quad (140)$$

Hence both  $\lambda^{\text{off}}$  and  $\lambda_t^*$  achieve the same principal order  $\sqrt{A_T T}$ , with  $\lambda_t^*$  adapting to non-uniform variation patterns.

## I. Two summation inequalities used in the online schedule analysis

Let  $\hat{\alpha}_1^T$  be a nonnegative sequence (an online proxy of nonstationarity), and define prefix sums

$$\hat{A}_t := \sum_{i=1}^t \hat{\alpha}_i, \quad \hat{A}_0 := 0. \quad (141)$$

To avoid division by zero, adopt the convention: if  $\hat{A}_t = 0$ , then  $\hat{\alpha}_t = 0$ , and any expression  $\hat{\alpha}_t/\sqrt{\hat{A}_t}$  is interpreted as 0.

### I.1. Square-root potential trick

**Lemma I.1.** *For any nonnegative sequence  $\hat{\alpha}_t$  and  $\hat{A}_t$  as in (H.1),*

$$\sum_{t=1}^T \frac{\hat{\alpha}_t}{\sqrt{\hat{A}_t}} \leq 2\sqrt{\hat{A}_T}. \quad (142)$$

*Proof.* For any  $t$  with  $\hat{A}_t > 0$ ,

$$\sqrt{\hat{A}_t} - \sqrt{\hat{A}_{t-1}} \frac{\hat{A}_t - \hat{A}_{t-1}}{\sqrt{\hat{A}_t} + \sqrt{\hat{A}_{t-1}}} \frac{\hat{\alpha}_t}{\sqrt{\hat{A}_t} + \sqrt{\hat{A}_{t-1}}} \geq \frac{\hat{\alpha}_t}{2\sqrt{\hat{A}_t}}. \quad (143)$$

Rearranging gives  $\hat{\alpha}_t/\sqrt{\hat{A}_t} \leq 2(\sqrt{\hat{A}_t} - \sqrt{\hat{A}_{t-1}})$ . Summing telescopes to  $2\sqrt{\hat{A}_T}$ .  $\square$

### I.2. Bounding $\sum_t \sqrt{\hat{A}_t/t}$

**Lemma I.2.** *For any nonnegative sequence  $\hat{\alpha}_t$  and  $\hat{A}_t$  as in (H.1),*

$$\sum_{t=1}^T \sqrt{\frac{\hat{A}_t}{t}} \leq 2\sqrt{T\hat{A}_T}. \quad (144)$$

*Proof.* Since  $\hat{A}_t$  is nondecreasing,  $\hat{A}_t \leq \hat{A}_T$  for all  $t$ , hence

$$\sum_{t=1}^T \sqrt{\frac{\hat{A}_t}{t}} \leq \sqrt{\hat{A}_T} \sum_{t=1}^T \frac{1}{\sqrt{t}}. \quad (145)$$

Using the integral comparison  $\sum_{t=1}^T t^{-1/2} \leq 1 + \int_1^T x^{-1/2} dx = 1 + 2(\sqrt{T} - 1) \leq 2\sqrt{T}$  yields (H.3).  $\square$

## J. Clipping $\lambda_t$ to $[\lambda_{\min}, \lambda_{\max}]$ : Effects and Compensation Terms

### J.1. Clipping introduces only controllable additive terms

Suppose an online scheduler produces a “raw” temperature  $\lambda_t^{\text{raw}} > 0$ , and the implementation clips it to

$$\lambda_t := \Pi_{[\lambda_{\min}, \lambda_{\max}]}(\lambda_t^{\text{raw}}) \min \lambda_{\max}, \max \lambda_{\min}, \lambda_t^{\text{raw}}. \quad (146)$$

This appendix shows that replacing  $\lambda_t^{\text{raw}}$  by  $\lambda_t$  preserves the main trade-off bound, up to an additive endpoint compensation term.

#### J.1.1. POINTWISE INEQUALITIES

Since  $\widehat{\alpha}_t \geq 0$ , the map  $\lambda \mapsto \widehat{\alpha}_t/\lambda$  is decreasing on  $\lambda > 0$ , while  $\lambda \mapsto \lambda$  is increasing. The following two pointwise bounds suffice:

**Lemma J.1.** *For any  $t$ ,*

$$\frac{\widehat{\alpha}_t}{\lambda_t} \leq \frac{\widehat{\alpha}_t}{\lambda_t^{\text{raw}}} + \frac{\widehat{\alpha}_t}{\lambda_{\max}}, \quad (147)$$

and

$$\lambda_t \leq \lambda_t^{\text{raw}} + \lambda_{\min}. \quad (148)$$

*Proof.* If  $\lambda_t^{\text{raw}} \leq \lambda_{\max}$ , then  $\lambda_t \geq \lambda_t^{\text{raw}}$ , hence  $\widehat{\alpha}_t/\lambda_t \leq \widehat{\alpha}_t/\lambda_t^{\text{raw}}$ . If  $\lambda_t^{\text{raw}} > \lambda_{\max}$ , then  $\lambda_t = \lambda_{\max}$  and  $\widehat{\alpha}_t/\lambda_t = \widehat{\alpha}_t/\lambda_{\max} \leq \widehat{\alpha}_t/\lambda_t^{\text{raw}} + \widehat{\alpha}_t/\lambda_{\max}$ .

If  $\lambda_t^{\text{raw}} \geq \lambda_{\min}$ , then  $\lambda_t \leq \lambda_t^{\text{raw}}$ , so  $\lambda_t \leq \lambda_t^{\text{raw}} + \lambda_{\min}$ . If  $\lambda_t^{\text{raw}} < \lambda_{\min}$ , then  $\lambda_t = \lambda_{\min} \leq \lambda_t^{\text{raw}} + \lambda_{\min}$ .  $\square$

#### J.1.2. SUMMING YIELDS THE COMPENSATION TERM

Multiply 147- 148 by constants  $C_1, C_2$  and sum:

$$\sum_{t=1}^T C_1 \frac{\widehat{\alpha}_t}{\lambda_t} \leq \sum_{t=1}^T C_1 \frac{\widehat{\alpha}_t}{\lambda_t^{\text{raw}}} + \sum_{t=1}^T C_1 \frac{\widehat{\alpha}_t}{\lambda_{\max}} \sum_{t=1}^T C_1 \frac{\widehat{\alpha}_t}{\lambda_t^{\text{raw}}} + \frac{C_1 \widehat{A}_T}{\lambda_{\max}}, \quad (149)$$

$$\sum_{t=1}^T C_2 \lambda_t \leq \sum_{t=1}^T C_2 \lambda_t^{\text{raw}} + \sum_{t=1}^T C_2 \lambda_{\min} \sum_{t=1}^T C_2 \lambda_t^{\text{raw}} + C_2 T \lambda_{\min}. \quad (150)$$

Adding gives

$$\sum_{t=1}^T \left( C_1 \frac{\widehat{\alpha}_t}{\lambda_t} + C_2 \lambda_t \right) \leq \sum_{t=1}^T \left( C_1 \frac{\widehat{\alpha}_t}{\lambda_t^{\text{raw}}} + C_2 \lambda_t^{\text{raw}} \right) + \frac{C_1 \widehat{A}_T}{\lambda_{\max}} + C_2 T \lambda_{\min}. \quad (151)$$

Thus clipping preserves the main bound and introduces only the controllable additive endpoints  $\frac{C_1 \widehat{A}_T}{\lambda_{\max}} + C_2 T \lambda_{\min}$ .

If the main bound includes an initial term such as  $D_{\Psi}(u_1, x_1)/\eta_1$ , then  $\lambda_1 \geq \lambda_{\min}$  (hence  $\eta_1 = c\lambda_1 \geq c\lambda_{\min}$ ) implies this initial term is also bounded by a constant, e.g.,  $\log K/(c\lambda_{\min})$  as in Appendix G.

## J.2. Why clipping is necessary in RL implementations (stability principles)

In continuous-control off-policy algorithms, the proxy  $\widehat{\alpha}_t$  (e.g., critic drift, TD-residual-based surrogates) is noisy and can exhibit: (i) **spikes**, which would drive  $\lambda_t$  excessively large and destabilize both the actor entropy regularization and the critic target scaling; and (ii) **near-zero plateaus**, which would collapse  $\lambda_t$  toward 0, making the policy nearly deterministic, harming exploration and adaptation when the environment changes.

Therefore, clipping is not an ad hoc heuristic: it is a stabilization step that turns an idealized scheduler into a numerically trainable system. The theory above formalizes that clipping changes only constants and adds a transparent endpoint compensation term.

## K. Soft Bellman Operator and Sensitivity of $Q^*$ (Proof of Eq. (25))

This appendix establishes a Lipschitz-type sensitivity bound for the soft-optimal action-value function under one-step MDP perturbations. Consider the discounted soft MDP at round  $t$ ,

$$\mathcal{M}_t := (\mathcal{S}, \mathcal{A}, P_t, r_t, \gamma), \quad \gamma \in (0, 1), \quad (152)$$

with entropy weight  $\mu > 0$ . For notational simplicity,  $\mathcal{A}$  is assumed finite in this appendix.

### K.1. Soft Bellman optimality operator (log-sum-exp form)

For any  $Q : \mathcal{S} \times \mathcal{A} \rightarrow \mathbb{R}$ , define the induced soft state-value

$$V_Q(s) := \mu \log \sum_{a \in \mathcal{A}} \exp\left(\frac{Q(s, a)}{\mu}\right). \quad (153)$$

The soft Bellman optimality operator at round  $t$  is

$$(\mathcal{T}_t Q)(s, a) := r_t(s, a) + \gamma \mathbb{E}_{s' \sim P_t(\cdot | s, a)}[V_Q(s')], \quad \forall (s, a) \in \mathcal{S} \times \mathcal{A}. \quad (154)$$

The soft-optimal action-value  $Q_t^*$  is the unique fixed point:

$$Q_t^* = \mathcal{T}_t Q_t^*. \quad (155)$$

### K.2. A key lemma: log-sum-exp is 1-Lipschitz in $\|\cdot\|_\infty$

**Lemma K.1** (Log-sum-exp is 1-Lipschitz under  $\|\cdot\|_\infty$ ). *For any  $x, y \in \mathbb{R}^{|\mathcal{A}|}$  and any  $\mu > 0$ ,*

$$\left| \mu \log \sum_a e^{x_a/\mu} - \mu \log \sum_a e^{y_a/\mu} \right| \leq \|x - y\|_\infty. \quad (156)$$

Consequently, for any  $Q, Q'$  and any  $s \in \mathcal{S}$ ,

$$|V_Q(s) - V_{Q'}(s)| \leq \|Q(s, \cdot) - Q'(s, \cdot)\|_\infty \leq \|Q - Q'\|_\infty. \quad (157)$$

*Proof.* Let  $g(z) := \mu \log \sum_a e^{z_a/\mu}$ . Then  $\nabla g(z) = \text{softmax}(z/\mu)$  has nonnegative coordinates summing to 1, hence  $\|\nabla g(z)\|_1 = 1$ . By the mean value theorem,  $g(x) - g(y) = \langle \nabla g(\xi), x - y \rangle$  for some  $\xi$  on the segment between  $x$  and  $y$ . Hölder's inequality yields  $|g(x) - g(y)| \leq \|\nabla g(\xi)\|_1 \|x - y\|_\infty = \|x - y\|_\infty$ . Applying this pointwise to  $x = Q(s, \cdot)$  and  $y = Q'(s, \cdot)$  gives (157).  $\square$

### K.3. $\mathcal{T}_t$ is a $\gamma$ -contraction in $\|\cdot\|_\infty$

**Lemma K.2** ( $\gamma$ -contraction). *For any  $t$  and any  $Q, Q'$ ,*

$$\|\mathcal{T}_t Q - \mathcal{T}_t Q'\|_\infty \leq \gamma \|Q - Q'\|_\infty. \quad (158)$$

*Proof.* Fix  $(s, a)$ . By (154) and (157),

$$|(\mathcal{T}_t Q)(s, a) - (\mathcal{T}_t Q')(s, a)| = \gamma \left| \mathbb{E}_{P_t(\cdot | s, a)}[V_Q(s') - V_{Q'}(s')] \right| \leq \gamma \|Q - Q'\|_\infty.$$

Taking the supremum over  $(s, a)$  proves (158).  $\square$

### K.4. Bounding $\|\mathcal{T}_t Q - \mathcal{T}_{t-1} Q\|_\infty$ via reward and transition drift

Define one-step MDP drift quantities

$$\Delta_t^r := \|r_t - r_{t-1}\|_\infty = \sup_{s, a} |r_t(s, a) - r_{t-1}(s, a)|, \quad (159)$$

$$\Delta_t^P := \sup_{s, a} \|P_t(\cdot | s, a) - P_{t-1}(\cdot | s, a)\|_1. \quad (160)$$

Let  $V_{\max}(Q) := \|V_Q\|_\infty = \sup_s |V_Q(s)|$ .

**Lemma K.3** (Operator drift bound). *For any  $Q$ ,*

$$\|\mathcal{T}_t Q - \mathcal{T}_{t-1} Q\|_\infty \leq \Delta_t^r + \gamma V_{\max}(Q) \Delta_t^P. \quad (161)$$

*Proof.* Fix  $(s, a)$ . Using (154),

$$|(\mathcal{T}_t Q)(s, a) - (\mathcal{T}_{t-1} Q)(s, a)| \leq |r_t(s, a) - r_{t-1}(s, a)| + \gamma \left| \mathbb{E}_{P_t}[V_Q] - \mathbb{E}_{P_{t-1}}[V_Q] \right|.$$

The first term is bounded by  $\Delta_t^r$ . For the second term, the standard inequality for bounded  $f$  and distributions  $p, q$ ,  $|\mathbb{E}_p[f] - \mathbb{E}_q[f]| \leq \|f\|_\infty \|p - q\|_1$ , implies

$$\left| \mathbb{E}_{P_t(\cdot|s,a)}[V_Q] - \mathbb{E}_{P_{t-1}(\cdot|s,a)}[V_Q] \right| \leq \|V_Q\|_\infty \|P_t(\cdot|s,a) - P_{t-1}(\cdot|s,a)\|_1 \leq V_{\max}(Q) \Delta_t^P.$$

Taking the supremum over  $(s, a)$  yields (161).  $\square$

### K.5. Fixed-point perturbation for contractions

**Lemma K.4** (Fixed-point sensitivity for  $\gamma$ -contractions). *Let  $\mathcal{T}$  and  $\mathcal{S}$  be  $\gamma$ -contractions under  $\|\cdot\|_\infty$  with unique fixed points  $Q^\mathcal{T} = \mathcal{T}Q^\mathcal{T}$  and  $Q^\mathcal{S} = \mathcal{S}Q^\mathcal{S}$ . Then*

$$\|Q^\mathcal{T} - Q^\mathcal{S}\|_\infty \leq \frac{1}{1-\gamma} \|\mathcal{T}Q^\mathcal{S} - \mathcal{S}Q^\mathcal{S}\|_\infty. \quad (162)$$

*Proof.*

$$\|Q^\mathcal{T} - Q^\mathcal{S}\|_\infty = \|\mathcal{T}Q^\mathcal{T} - \mathcal{S}Q^\mathcal{S}\|_\infty \leq \|\mathcal{T}Q^\mathcal{T} - \mathcal{T}Q^\mathcal{S}\|_\infty + \|\mathcal{T}Q^\mathcal{S} - \mathcal{S}Q^\mathcal{S}\|_\infty \leq \gamma \|Q^\mathcal{T} - Q^\mathcal{S}\|_\infty + \|\mathcal{T}Q^\mathcal{S} - \mathcal{S}Q^\mathcal{S}\|_\infty.$$

Rearranging gives (162).  $\square$

### K.6. Sensitivity of $Q_t^*$ (Proof of Eq. (25))

Applying Lemma K.4 with  $\mathcal{T} = \mathcal{T}_t$ ,  $\mathcal{S} = \mathcal{T}_{t-1}$ , and  $Q^\mathcal{S} = Q_{t-1}^*$  yields

$$\|Q_t^* - Q_{t-1}^*\|_\infty \leq \frac{1}{1-\gamma} \|\mathcal{T}_t Q_{t-1}^* - \mathcal{T}_{t-1} Q_{t-1}^*\|_\infty. \quad (163)$$

Then Lemma K.3 (with  $Q = Q_{t-1}^*$ ) implies

$$\|\mathcal{T}_t Q_{t-1}^* - \mathcal{T}_{t-1} Q_{t-1}^*\|_\infty \leq \Delta_t^r + \gamma V_{\max}(Q_{t-1}^*) \Delta_t^P. \quad (164)$$

Combining (163)–(164) gives the desired reward-plus-transition sensitivity bound:

$$\boxed{\|Q_t^* - Q_{t-1}^*\|_\infty \leq \frac{1}{1-\gamma} \left( \Delta_t^r + \gamma V_{\max}(Q_{t-1}^*) \Delta_t^P \right)}. \quad (165)$$

**Optional explicit bound on  $V_{\max}(Q_t^*)$ .** If rewards are bounded as  $|r_t(s, a)| \leq R_{\max}$ , then standard arguments yield

$$\|Q_t^*\|_\infty \leq \frac{R_{\max} + \gamma \mu \log |\mathcal{A}|}{1-\gamma}, \quad \|V_{Q_t^*}\|_\infty \leq \frac{R_{\max} + \mu \log |\mathcal{A}|}{1-\gamma}. \quad (166)$$

Substituting (166) into (165) makes the bound depend only on  $\Delta_t^r, \Delta_t^P, \gamma, \mu, |\mathcal{A}|$ .

### L. Softmax Lipschitzness (Statewise RL Formulation) (Proof of Eq. (26))

This appendix records a standard Lipschitz bound for the Boltzmann/softmax mapping, specialized to the statewise policy map in soft RL.

### L.1. Jacobian and the $\ell_\infty \rightarrow \ell_1$ operator norm

Assume  $|\mathcal{A}| = K < \infty$ . For  $q \in \mathbb{R}^K$ , define  $\pi(q) = \text{softmax}(q/\mu)$  by

$$\pi(q)_i = \frac{\exp(q_i/\mu)}{\sum_{j=1}^K \exp(q_j/\mu)}, \quad i \in [K],$$

where  $\mu > 0$  is the temperature (entropy weight). A direct differentiation gives

$$\frac{\partial \pi_i(q)}{\partial q_j} = \frac{1}{\mu} \pi_i(q) (\mathbf{1}\{i=j\} - \pi_j(q)),$$

hence

$$\nabla \pi(q) = \frac{1}{\mu} \left( \text{Diag}(\pi(q)) - \pi(q) \pi(q)^\top \right). \quad (167)$$

Define the operator norm

$$\|\nabla \pi(q)\|_{\infty \rightarrow 1} := \sup_{\|h\|_\infty \leq 1} \|\nabla \pi(q)h\|_1.$$

Let  $\pi = \pi(q)$  and consider any  $h$  with  $\|h\|_\infty \leq 1$ . The vector  $(\text{Diag}(\pi) - \pi\pi^\top)h$  has coordinates  $\pi_i(h_i - \mathbb{E}_\pi[h])$ , thus

$$\|(\text{Diag}(\pi) - \pi\pi^\top)h\|_1 = \sum_{i=1}^K \pi_i |h_i - \mathbb{E}_\pi[h]| = \mathbb{E}_\pi[|H - \mathbb{E}H|], \quad (168)$$

where  $H$  is the random variable taking value  $h_I$  with  $I \sim \pi$ . Since  $H \in [-1, 1]$ ,  $\text{Var}(H) \leq 1$ , and by Cauchy–Schwarz,

$$\mathbb{E}[|H - \mathbb{E}H|] \leq \sqrt{\mathbb{E}(H - \mathbb{E}H)^2} = \sqrt{\text{Var}(H)} \leq 1. \quad (169)$$

Combining (167)–(169) yields

$$\|\nabla \pi(q)\|_{\infty \rightarrow 1} \leq \frac{1}{\mu}. \quad (170)$$

This bound is tight (e.g.,  $K = 2$  and  $\pi = (1/2, 1/2)$ ).

### L.2. Global Lipschitzness and the statewise form

By the mean value theorem applied to the vector map  $\pi(\cdot)$  and (170), for any  $q, q' \in \mathbb{R}^K$ ,

$$\|\pi(q) - \pi(q')\|_1 \leq \frac{1}{\mu} \|q - q'\|_\infty. \quad (171)$$

In soft RL, for each state  $s$ , define  $q(s) := Q(s, \cdot) \in \mathbb{R}^K$  and the Boltzmann policy

$$\pi_Q(\cdot | s) := \text{softmax}(Q(s, \cdot)/\mu) = \pi(q(s)).$$

Applying (171) statewise yields, for any  $s$ ,

$$\|\pi_Q(\cdot | s) - \pi_{Q'}(\cdot | s)\|_1 \leq \frac{1}{\mu} \|Q(s, \cdot) - Q'(s, \cdot)\|_\infty \leq \frac{1}{\mu} \|Q - Q'\|_\infty. \quad (172)$$

In particular, taking  $Q = Q_t^*$  and  $Q' = Q_{t-1}^*$  gives the policy-drift bound stated as Eq. (26) in the main text:

$$\|\pi_t^*(\cdot | s) - \pi_{t-1}^*(\cdot | s)\|_1 \leq \frac{1}{\mu} \|Q_t^* - Q_{t-1}^*\|_\infty.$$

**Remark (constant  $\mu$  across states).** The Lipschitz constant in (172)–(173) equals  $1/\mu$ . Allowing state-dependent temperatures  $\mu(s)$  would introduce non-uniform constants  $\max_s 1/\mu(s)$  (or more intricate weighted constants) when aggregating statewise bounds. A single global  $\mu$  preserves a clean uniform constant in the  $Q^* \rightarrow \pi^*$  drift transfer.

## M. From Squared Drift to Variation: Why a Constant $C_Q$ is Needed

A recurring step in connecting statewise squared policy drifts to a linear MDP-variation budget is to convert  $\sum_t \|\Delta Q_t^*\|_\infty^2$  into  $\sum_t \|\Delta Q_t^*\|_\infty$ . This appendix provides an explicit constant  $C_Q$  ensuring

$$\sum_{t=2}^T \|\Delta Q_t^*\|_\infty^2 \leq C_Q \sum_{t=2}^T \|\Delta Q_t^*\|_\infty, \quad \Delta Q_t^* := Q_t^* - Q_{t-1}^*. \quad (174)$$

### M.1. An explicit $C_Q$ from boundedness of $Q_t^*$

Assume bounded rewards:

$$|r_t(s, a)| \leq R_{\max}, \quad \forall t, s, a. \quad (175)$$

**Lemma M.1** (Uniform  $\ell_\infty$  bound for soft-optimal  $Q_t^*$ ). *Under (175),*

$$\|Q_t^*\|_\infty \leq Q_{\max} := \frac{R_{\max} + \gamma \mu \log |\mathcal{A}|}{1 - \gamma}, \quad \forall t. \quad (176)$$

*Proof sketch.* For any state  $s$ ,  $V_{Q_t^*}(s) \leq \max_a Q_t^*(s, a) + \mu \log |\mathcal{A}|$  by (153). Let  $M_t := \|Q_t^*\|_\infty$ . From the fixed point equation (155),

$$M_t \leq R_{\max} + \gamma(M_t + \mu \log |\mathcal{A}|),$$

which rearranges to (176).  $\square$

By (176),

$$\|\Delta Q_t^*\|_\infty \leq \|Q_t^*\|_\infty + \|Q_{t-1}^*\|_\infty \leq 2Q_{\max}, \quad \forall t \geq 2. \quad (177)$$

Therefore,

$$\sum_{t=2}^T \|\Delta Q_t^*\|_\infty^2 \leq \left( \max_{t \geq 2} \|\Delta Q_t^*\|_\infty \right) \sum_{t=2}^T \|\Delta Q_t^*\|_\infty \leq (2Q_{\max}) \sum_{t=2}^T \|\Delta Q_t^*\|_\infty. \quad (178)$$

Hence (174) holds with the explicit choice

$$C_Q := 2Q_{\max} = \frac{2(R_{\max} + \gamma \mu \log |\mathcal{A}|)}{1 - \gamma}. \quad (179)$$

### M.2. Why (174) prevents a rate deterioration

A typical chain of bounds proceeds as follows.

**Step 1 (policy drift from  $Q^*$  drift).** Appendix L implies, statewise,

$$\|\pi_t^*(\cdot | s) - \pi_{t-1}^*(\cdot | s)\|_1 \leq \frac{1}{\mu} \|\Delta Q_t^*\|_\infty. \quad (180)$$

Thus squared policy drift satisfies

$$\alpha_{t,s} := \|\pi_t^*(\cdot | s) - \pi_{t-1}^*(\cdot | s)\|_1^2 \leq \frac{1}{\mu^2} \|\Delta Q_t^*\|_\infty^2. \quad (181)$$

**Step 2 (AES/OCO main term depends on a sum of squares).** The OCO/AES regret term (up to logs and constants) typically scales like

$$\text{Reg}_T \lesssim \sqrt{T \sum_{t,s} \alpha_{t,s}}. \quad (182)$$

Hence controlling  $\sum_t \|\Delta Q_t^*\|_\infty^2$  is essential via (181).

**Step 3 (MDP variation naturally controls a linear sum).** The soft Bellman sensitivity bounds in Appendix K yield linear-variation control of the form

$$\sum_{t=2}^T \|\Delta Q_t^*\|_\infty \lesssim B_T^{\text{MDP}}, \quad (183)$$

where  $B_T^{\text{MDP}}$  is a linear budget built from  $\sum_t \Delta_t^r$  and  $\sum_t \Delta_t^P$  (cf. (159)–(160)).

**Step 4 (why  $C_Q$  is needed).** Without (174), a crude bound  $\sum x_t^2 \leq (\sum x_t)^2$  would imply  $\sum_t \|\Delta Q_t^*\|_\infty^2 \leq (B_T^{\text{MDP}})^2$ , and substituting into (182) produces a deteriorated rate  $\text{Reg}_T \lesssim B_T^{\text{MDP}} \sqrt{T}$ . In contrast, (174) gives

$$\sum_{t=2}^T \|\Delta Q_t^*\|_\infty^2 \leq C_Q \sum_{t=2}^T \|\Delta Q_t^*\|_\infty \lesssim C_Q B_T^{\text{MDP}}, \quad (184)$$

and (182) recovers the intended  $\tilde{O}(\sqrt{B_T^{\text{MDP}} T})$  scaling:

$$\text{Reg}_T \lesssim \sqrt{T \cdot C_Q B_T^{\text{MDP}}} \asymp \sqrt{B_T^{\text{MDP}} T}, \quad (185)$$

where  $C_Q$  only affects constants.

## N. A Strict Decomposition of $J_t$ and Formal Definitions of Error Terms

This appendix provides a strict (identity-level) decomposition of the soft return gap and clarifies the origin and definition of the error terms (bias and occupancy mismatch) that arise when interfacing RL with a per-state OCO surrogate.

### N.1. Notation: discounted occupancy and maximum-entropy return

Fix  $\mathcal{M}_t = (\mathcal{S}, \mathcal{A}, P_t, r_t, \gamma)$ . For a policy  $\pi$ , define the discounted state occupancy

$$d_t^\pi(s) := (1 - \gamma) \sum_{h \geq 0} \gamma^h \Pr(s_h = s \mid \pi, P_t, \rho), \quad (186)$$

where  $\rho$  is the initial state distribution. For any measurable  $g(s, a)$ ,

$$\frac{1}{1 - \gamma} \mathbb{E}_{s \sim d_t^\pi, a \sim \pi(\cdot | s)}[g(s, a)] = \mathbb{E}\left[\sum_{h \geq 0} \gamma^h g(s_h, a_h)\right]. \quad (187)$$

The soft objective is

$$J_t(\pi) := \frac{1}{1 - \gamma} \mathbb{E}_{s \sim d_t^\pi, a \sim \pi(\cdot | s)}[r_t(s, a) - \mu \log \pi(a \mid s)]. \quad (188)$$

Define the soft policy-evaluation quantities:

$$\begin{aligned} Q_t^\pi(s, a) &:= r_t(s, a) + \gamma \mathbb{E}_{s' \sim P_t(\cdot | s, a)}[V_t^\pi(s')], \\ V_t^\pi(s) &:= \mathbb{E}_{a \sim \pi(\cdot | s)}[Q_t^\pi(s, a) - \mu \log \pi(a \mid s)]. \end{aligned} \quad (189)$$

Define the regularized advantage

$$\tilde{A}_t^\pi(s, a) := Q_t^\pi(s, a) - \mu \log \pi(a \mid s) - V_t^\pi(s), \quad (190)$$

which satisfies  $\mathbb{E}_{a \sim \pi(\cdot | s)}[\tilde{A}_t^\pi(s, a)] = 0$  for all  $s$ .

## N.2. Soft performance difference lemma (identity)

**Lemma N.1** (Soft (regularized) performance difference lemma). *For any two policies  $\pi, \pi'$ ,*

$$J_t(\pi') - J_t(\pi) = \frac{1}{1-\gamma} \mathbb{E}_{s \sim d_t^{\pi'}} \left[ \mathbb{E}_{a \sim \pi'(\cdot|s)} [\tilde{A}_t^{\pi}(s, a)] - \mu \text{KL}(\pi'(\cdot|s) \parallel \pi(\cdot|s)) \right]. \quad (191)$$

*Proof.* Define the soft Bellman operator for policy  $\pi'$  acting on a value function  $V$ :

$$(\mathcal{T}_t^{\pi'} V)(s) := \mathbb{E}_{a \sim \pi'(\cdot|s)} [r_t(s, a) - \mu \log \pi'(a|s) + \gamma \mathbb{E}_{s' \sim P_t(\cdot|s, a)} V(s')].$$

Then  $V_t^{\pi'}$  is its fixed point. Using the linear system representation,

$$V_t^{\pi'} - V_t^{\pi} = (I - \gamma P_t^{\pi'})^{-1} (\mathcal{T}_t^{\pi'} V_t^{\pi} - V_t^{\pi}),$$

and taking expectation over  $s_0 \sim \rho$  together with the occupancy identity (187) gives

$$J_t(\pi') - J_t(\pi) = \frac{1}{1-\gamma} \mathbb{E}_{s \sim d_t^{\pi'}} [(\mathcal{T}_t^{\pi'} V_t^{\pi})(s) - V_t^{\pi}(s)]. \quad (192)$$

Moreover,

$$(\mathcal{T}_t^{\pi'} V_t^{\pi})(s) = \mathbb{E}_{a \sim \pi'(\cdot|s)} [Q_t^{\pi}(s, a) - \mu \log \pi'(a|s)], \quad V_t^{\pi}(s) = \mathbb{E}_{a \sim \pi(\cdot|s)} [Q_t^{\pi}(s, a) - \mu \log \pi(a|s)].$$

Add and subtract  $-\mu \log \pi(a|s)$  inside the  $\pi'$ -expectation and use (190):

$$(\mathcal{T}_t^{\pi'} V_t^{\pi})(s) - V_t^{\pi}(s) = \mathbb{E}_{a \sim \pi'(\cdot|s)} [\tilde{A}_t^{\pi}(s, a)] + \mu \mathbb{E}_{a \sim \pi'(\cdot|s)} [\log \pi(a|s) - \log \pi'(a|s)] = \mathbb{E}_{a \sim \pi'} [\tilde{A}_t^{\pi}] - \mu \text{KL}(\pi' \parallel \pi).$$

Substituting into (192) yields (191).  $\square$

## N.3. A per-state convex surrogate and the inevitability of bias terms

The OCO interface uses the ideal per-state surrogate (defined using  $Q_t^*$ ):

$$f_{t,s}(\pi_s) := -\langle Q_t^*(s, \cdot), \pi_s \rangle + \mu \sum_a \pi_s(a) \log \pi_s(a). \quad (193)$$

Let  $\pi_t^*(\cdot|s) = \text{softmax}(Q_t^*(s, \cdot)/\mu)$ . Then:

**Lemma N.2** (Fenchel–Young identity: surrogate gap equals  $\mu \cdot \text{KL}$ ). *For any state  $s$  and any distribution  $\pi(\cdot|s)$ ,*

$$f_{t,s}(\pi(\cdot|s)) - f_{t,s}(\pi_t^*(\cdot|s)) = \mu \text{KL}(\pi(\cdot|s) \parallel \pi_t^*(\cdot|s)). \quad (194)$$

This identity is the key for translating soft RL into per-state strongly convex OCO losses. However, Lemma N.1 decomposes  $J_t(\pi_t^*) - J_t(\pi_t)$  using (i) the optimal occupancy  $d_t^{\pi_t^*}$ , (ii) the regularized advantage  $\tilde{A}_t^{\pi_t^*}$  (which depends on  $Q_t^{\pi_t^*}$ ), and (iii) the reverse-direction KL term  $\text{KL}(\pi_t^* \parallel \pi_t)$ . In contrast, (194) uses  $Q_t^*$  and the forward KL  $\text{KL}(\pi_t \parallel \pi_t^*)$ , and implementations may further replace  $Q_t^*$  by a critic estimate. Consequently, additional error terms are unavoidable when the strict RL identity is expressed in the surrogate form.

## N.4. Formal definitions of bias and occupancy mismatch

Introduce a “planning-style” objective that evaluates  $\pi$  under the optimal occupancy and  $Q_t^*$ :

$$\tilde{J}_t(\pi) := \frac{1}{1-\gamma} \mathbb{E}_{s \sim d_t^{\pi_t^*}, a \sim \pi(\cdot|s)} [Q_t^*(s, a) - \mu \log \pi(a|s)]. \quad (195)$$

By definition,  $J_t(\pi_t^*) = \tilde{J}_t(\pi_t^*)$ . Moreover, combining Lemma N.2 with (195) gives the exact “main term” identity

$$J_t(\pi_t^*) - \tilde{J}_t(\pi_t) = \frac{1}{1-\gamma} \mathbb{E}_{s \sim d_t^{\pi_t^*}} [f_{t,s}(\pi_t(\cdot|s)) - f_{t,s}(\pi_t^*(\cdot|s))] = \frac{\mu}{1-\gamma} \mathbb{E}_{s \sim d_t^{\pi_t^*}} \text{KL}(\pi_t(\cdot|s) \parallel \pi_t^*(\cdot|s)). \quad (196)$$

The true return gap decomposes as

$$J_t(\pi_t^*) - J_t(\pi_t) = \underbrace{(J_t(\pi_t^*) - \tilde{J}_t(\pi_t))}_{\text{ideal OCO/planning main term}} + \underbrace{(\tilde{J}_t(\pi_t) - J_t(\pi_t))}_{\text{interface errors (bias, occupancy mismatch, estimation)}}. \quad (197)$$

The second bracket in (197) is the source of the bias terms and distribution-mismatch terms.

(i)  **$Q$ -substitution bias ( $Q_t^*$  vs.  $Q_t^{\pi_t}$ ).** Define

$$\text{Bias}_t^{(Q)} := \frac{1}{1-\gamma} \mathbb{E}_{s \sim d_t^{\pi_t^*}, a \sim \pi_t(\cdot|s)} [Q_t^*(s, a) - Q_t^{\pi_t}(s, a)]. \quad (198)$$

A direct bound is

$$|\text{Bias}_t^{(Q)}| \leq \frac{1}{1-\gamma} \|Q_t^* - Q_t^{\pi_t}\|_\infty. \quad (199)$$

In soft actor-critic with function approximation and bootstrapping,  $\|Q_t^* - Q_t^{\pi_t}\|_\infty$  need not vanish; the main theorem therefore keeps  $\sum_t \text{Bias}_t^{(Q)}$  as an explicit additive term, interpreted as approximation/evaluation error.

(ii) **Estimation error (critic estimate vs. target  $Q$ ).** If the algorithm uses a critic estimate  $\hat{Q}_t$  (or a target network), an additional error may be tracked, e.g.

$$\text{Bias}_t^{(\text{est})} := \frac{1}{1-\gamma} \mathbb{E}_{s \sim d_t^{\pi_t^*}, a \sim \pi_t(\cdot|s)} [\hat{Q}_t(s, a) - Q_t^*(s, a)], \quad |\text{Bias}_t^{(\text{est})}| \leq \frac{1}{1-\gamma} \|\hat{Q}_t - Q_t^*\|_\infty. \quad (200)$$

(iii) **Occupancy mismatch.** If the analysis or implementation uses a substitute state distribution  $\tilde{d}_t$  (e.g. on-policy  $d_t^{\pi_t}$  or a replay-buffer distribution), define

$$\phi_t(s) := f_{t,s}(\pi_t(\cdot|s)) - f_{t,s}(\pi_t^*(\cdot|s)) (\geq 0), \quad \text{OccErr}_t(\tilde{d}_t) := \frac{1}{1-\gamma} \left( \mathbb{E}_{s \sim d_t^{\pi_t^*}} [\phi_t(s)] - \mathbb{E}_{s \sim \tilde{d}_t} [\phi_t(s)] \right). \quad (201)$$

The standard bound is

$$|\text{OccErr}_t(\tilde{d}_t)| \leq \frac{1}{1-\gamma} \|\phi_t\|_\infty \|d_t^{\pi_t^*} - \tilde{d}_t\|_1. \quad (202)$$

## O. A Formal Error-Decomposition Lemma and Proof

This appendix states and proves a clean inequality separating the ideal per-state surrogate main term from the interface errors (bias and occupancy mismatch). It also provides explicit bounds that make the mismatch term directly usable.

### O.1. Occupancy form and soft performance difference lemma

The definitions (186)–(191) already yield the occupancy form

$$J_t(\pi) = \frac{1}{1-\gamma} \mathbb{E}_{s \sim d_t^\pi, a \sim \pi(\cdot|s)} [r_t(s, a) - \mu \log \pi(a|s)], \quad (203)$$

and the strict identity (Lemma N.1) can be reused as needed.

### O.2. A bias term that is directly controlled by $\|Q_t^{\pi_t} - Q_t^*\|_\infty$

A convenient scalar bias term arising from  $Q$ -substitution is

$$\text{Bias}_t^{(Q)} := \frac{1}{1-\gamma} \mathbb{E}_{s \sim d_t^{\pi_t^*}, a \sim \pi_t^*(\cdot|s)} [Q_t^{\pi_t}(s, a) - Q_t^*(s, a)], \quad (204)$$

which admits the immediate bound

$$|\text{Bias}_t^{(Q)}| \leq \frac{1}{1-\gamma} \|Q_t^{\pi_t} - Q_t^*\|_\infty. \quad (205)$$

The main theorem can keep  $\sum_{t=1}^T |\text{Bias}_t^{(Q)}|$  explicit. Any rate claim beyond this requires additional assumptions on evaluation/approximation accuracy (e.g. a decay  $\|Q_t^{\pi_t} - Q_t^*\|_\infty = O(t^{-1/2})$  would imply an  $O(\sqrt{T})$  cumulative contribution).

### O.3. Occupancy mismatch: from distribution replacement to an $\ell_1$ bound

Recall the statewise surrogate gap

$$\Delta_t(s) := f_{t,s}(\pi_t(\cdot | s)) - f_{t,s}(\pi_t^*(\cdot | s)) \geq 0, \quad (206)$$

where

$$f_{t,s}(\pi_s) = -\langle Q_t^*(s, \cdot), \pi_s \rangle + \mu \sum_a \pi_s(a) \log \pi_s(a). \quad (207)$$

For any substitute distribution  $\tilde{d}_t$  define

$$\text{OccErr}_t(\tilde{d}_t) := \frac{1}{1-\gamma} \left( \mathbb{E}_{s \sim d_t^{\pi_t^*}} [\Delta_t(s)] - \mathbb{E}_{s \sim \tilde{d}_t} [\Delta_t(s)] \right). \quad (208)$$

Then, for bounded  $\Delta_t$ ,

$$|\text{OccErr}_t(\tilde{d}_t)| \leq \frac{1}{1-\gamma} \|\Delta_t\|_\infty \|d_t^{\pi_t^*} - \tilde{d}_t\|_1. \quad (209)$$

### O.4. An explicit bound on $\|\Delta_t\|_\infty$

Assume  $|r_t(s, a)| \leq R_{\max}$  so that  $\|Q_t^*\|_\infty \leq Q_{\max}$  with  $Q_{\max}$  defined in (176). Then for any fixed state  $s$  and any  $\pi_s \in \Delta_{\mathcal{A}}$ ,

$$-\langle Q_t^*(s, \cdot), \pi_s \rangle \in [-Q_{\max}, Q_{\max}], \quad \sum_a \pi_s(a) \log \pi_s(a) \in [-\log |\mathcal{A}|, 0].$$

Hence  $f_{t,s}(\pi_s) \in [-Q_{\max} - \mu \log |\mathcal{A}|, Q_{\max}]$ , so the difference between any two values is at most the interval length. Therefore,

$$0 \leq \Delta_t(s) \leq 2Q_{\max} + \mu \log |\mathcal{A}|, \quad \forall s, \quad (210)$$

and

$$\|\Delta_t\|_\infty \leq 2Q_{\max} + \mu \log |\mathcal{A}|. \quad (211)$$

Substituting (211) into (209) gives a fully explicit mismatch bound:

$$|\text{OccErr}_t(\tilde{d}_t)| \leq \frac{2Q_{\max} + \mu \log |\mathcal{A}|}{1-\gamma} \|d_t^{\pi_t^*} - \tilde{d}_t\|_1. \quad (212)$$

### O.5. Optional strengthening for on-policy weighting

When  $\tilde{d}_t = d_t^{\pi_t}$  (on-policy sampling), the occupancy distance can be further controlled by a uniform per-state policy difference. Define the induced state-transition kernel

$$P_t^\pi(s' | s) := \mathbb{E}_{a \sim \pi(\cdot | s)} [P_t(s' | s, a)], \quad (213)$$

and the mixed norm

$$\|\pi - \pi'\|_{1,\infty} := \sup_{s \in \mathcal{S}} \|\pi(\cdot | s) - \pi'(\cdot | s)\|_1. \quad (214)$$

Then the standard resolvent/telescoping argument yields

$$\|d_t^\pi - d_t^{\pi'}\|_1 \leq \frac{\gamma}{1-\gamma} \sup_s \|P_t^\pi(\cdot | s) - P_t^{\pi'}(\cdot | s)\|_1 \leq \frac{\gamma}{1-\gamma} \|\pi - \pi'\|_{1,\infty}. \quad (215)$$

Combining (212) and (215) gives an on-policy mismatch control in terms of  $\|\pi_t^* - \pi_t\|_{1,\infty}$ .

## P. Reproducibility and Experimental Protocol

This appendix provides implementation-level details required for reproducing the experimental results reported in the main paper. All conceptual motivations, algorithmic design choices, and evaluation rationales are described in the main text and are not repeated here.

### P.1. Scope of Algorithmic Modifications

Adaptive Entropy Scheduling (AES) does not introduce a new reinforcement learning algorithm. For all experiments, the underlying algorithmic carriers (SAC, PPO, SQL, and MEow) are used without modification to their policy parameterization, value functions, optimization objectives, or update rules.

The only modification relative to the baseline implementations is the replacement of a fixed entropy regularization weight with a time-varying scalar produced by the AES scheduler. No additional neural networks, auxiliary losses, replay mechanisms, or environment resets are introduced.

### P.2. Drift Proxy Computation

AES requires a scalar non-stationarity proxy at each update step. This proxy is computed exclusively from quantities already produced during standard training.

For off-policy methods (SAC, SQL, MEow), the proxy is computed from absolute temporal-difference (TD) errors of critic updates. For PPO, the proxy is computed from absolute TD deltas of the value function over the rollout batch.

Concretely, given a batch of errors  $\{\delta_i\}$ , the proxy is defined as the upper quantile

$$\hat{v}_t = \text{Quantile}_q(|\delta|), \quad q = 0.9.$$

An optional exponential moving average is applied for smoothing, with a fixed coefficient shared across all experiments. No task-specific or hand-crafted signals are used.

### P.3. Entropy Scheduling Details

The AES scheduler maps the accumulated drift proxy to an entropy weight using the closed-form rule derived in Section 3.

For numerical stability and reproducibility, the scheduled entropy weight is clipped to a fixed interval  $[\lambda_{\min}, \lambda_{\max}]$ . Clipping bounds are held constant across all tasks within the same algorithmic carrier.

The scheduled value directly replaces the original entropy coefficient used by the base algorithm (temperature for SAC/SQL/MEow, entropy bonus coefficient for PPO).

### P.4. Non-Stationarity Alignment

All methods are trained and evaluated under identical non-stationarity schedules. Environmental changes are aligned by environment interaction steps rather than wall-clock time.

For each task, the same change points, drift magnitudes, and evaluation intervals are used across all methods. AES does not modify environment dynamics, reset behavior, or termination conditions.

### P.5. Random Seeds and Statistical Protocol

Each experiment is repeated over multiple independent random seeds. Random seeds control environment initialization, network parameter initialization, minibatch sampling, and stochastic action sampling.

All reported curves and metrics are computed using identical evaluation code paths for baseline and AES-enhanced variants.

### P.6. Computational Overhead

AES introduces negligible computational overhead. Per update, it requires computing a single scalar statistic from existing TD errors and evaluating a lightweight closed-form schedule.

No additional forward or backward passes are introduced.

## Q. Ablation and Sensitivity Analysis

We conduct a set of ablation and sensitivity studies to assess the robustness of Adaptive Entropy Scheduling (AES) with respect to its key design choices, including drift proxies, coupling between optimization step size and entropy coefficient,

smoothing strength, and clipping ranges. Unless otherwise specified, all results are averaged across task families (Toy, MuJoCo, Isaac Gym) and drift patterns (abrupt, linear, periodic, mixed).

**Metrics.** We report normalized area under the return curve (nAUC, higher is better), drop-area ratio (lower is better), and normalized recovery time after distribution shifts (lower is better), following standard practice in non-stationary reinforcement learning.

### Q.1. Component Ablation

Table 4 evaluates the contribution of individual AES components. Removing AES entirely by fixing the entropy coefficient leads to substantial degradation across all metrics. Disabling either clipping or the coupling between the actor learning rate and the entropy coefficient results in consistently worse stability and slower recovery, indicating that both components contribute meaningfully to robust adaptation.

Alternative drift proxies based on mean TD error or value loss lead to inferior performance compared to quantile-based TD error, suggesting that these proxies are more sensitive to optimization noise. Using critic parameter drift yields performance comparable to the default proxy, though with slightly reduced recovery speed.

Table 4. Ablation of AES components. Results are averaged across tasks and drift patterns.

Variant	Proxy	Coupling	Clipping	nAUC $\uparrow$	Drop-area $\downarrow$
Fixed $\lambda$ (No AES)	–	–	–	0.78	0.31
AES (Default)	TD ( $q=0.8$ )	✓	✓	<b>0.84</b>	<b>0.19</b>
AES w/o coupling	TD ( $q=0.8$ )	✗	✓	0.82	0.22
AES w/o clipping	TD ( $q=0.8$ )	✓	✗	0.81	0.26
AES (TD mean)	TD mean	✓	✓	0.82	0.23
AES (value loss)	Value loss	✓	✓	0.81	0.24
AES (critic drift)	$\ \Delta\theta_Q\ $	✓	✓	0.83	0.21

### Q.2. Sensitivity to Quantile Level

Table 5 reports performance as a function of the TD-error quantile level  $q$ . Moderate-to-high quantiles ( $q \in [0.7, 0.9]$ ) achieve the best overall trade-off between stability and recovery. Lower quantiles underreact to distributional shifts, while very high quantiles introduce additional variance that negatively affects stability.

Table 5. Sensitivity to TD-error quantile  $q$  (AES, other settings fixed).

$q$	nAUC $\uparrow$	Drop-area $\downarrow$
0.5	0.82	0.23
0.7	0.83	0.21
0.8	<b>0.84</b>	<b>0.19</b>
0.9	0.83	0.20
0.95	0.81	0.25

### Q.3. Sensitivity to Smoothing Strength

Table 6 examines the effect of EMA smoothing on the drift proxy. Weak smoothing leads to increased variability and degraded stability, while overly strong smoothing delays adaptation to abrupt shifts, increasing recovery time. Intermediate smoothing values provide a favorable balance across metrics.

### Q.4. Sensitivity to Clipping Range

Table 7 evaluates the effect of different clipping ranges for the entropy coefficient. Excessively wide ranges increase instability, while overly restrictive ranges slow adaptation to abrupt changes. The default range achieves consistently strong performance across all metrics.

Table 6. Sensitivity to EMA smoothing coefficient  $\beta$  (AES,  $q = 0.8$ ).

EMA $\beta$	nAUC $\uparrow$	Drop-area $\downarrow$
0.80	0.82	0.24
0.90	0.83	0.21
0.95	<b>0.84</b>	<b>0.19</b>
0.98	0.83	0.18
0.99	0.82	0.18

Table 7. Sensitivity to entropy coefficient clipping range (AES).

$[\lambda_{\min}, \lambda_{\max}]$	nAUC $\uparrow$	Drop-area $\downarrow$
[0.01, 2.00]	0.82	0.25
[0.05, 1.00]	<b>0.84</b>	<b>0.19</b>
[0.10, 1.00]	0.83	0.19
[0.05, 0.50]	0.82	0.20
[0.10, 0.50]	0.80	0.22

## Q.5. Breakdown by Drift Type

Finally, Table 8 separates performance by drift category. AES provides the largest gains under abrupt shifts, particularly in recovery time, while also improving stability under gradual or periodic changes.

Table 8. Performance breakdown by drift type.

Drift Type	Method	nAUC $\uparrow$	Drop-area $\downarrow$
Abrupt	Fixed $\lambda$	0.71	0.41
Abrupt	AES	<b>0.80</b>	<b>0.23</b>
Non-abrupt	Fixed $\lambda$	0.81	0.26
Non-abrupt	AES	<b>0.85</b>	<b>0.18</b>